ACS OMEGA

http://pubs.acs.org/journal/acsodf

Article

Mineralogical and Geochemical Compositions of Ammonian Illite-Enriched High-Rank Coals of the Xingying Mine, Northeastern Chongqing, China

Jianhua Zou,* Hui Wang, Hongyu Chen, Hang Li, and Tian Li

Cite This: *ACS Omega* 2022, 7, 18969−18984

Read Online

ACCESS | Metrics & More | Article Recommendations

ABSTRACT: Ammonian illite (NH_4-illite)-rich late Permian coals of high rank were discovered in southwestern China. This research reports new mineralogical and geochemical data of 11 bench samples from the adjacent Xingying mine, northeastern Chongqing Coalfield, southwestern China, with an emphasis on the modes of occurrence and origin of NH_4-illite. The Xingying coals, with low ash yields and medium sulfur, have a high rank (semianthrite, $R_{o,ran}$ = 3.67%), owing to the plutonic metamorphism. Minerals in the coal consist of NH_4-illite and pyrite and, to a lesser extent, jarosite, albite, and anatase, with traces of chamosite, quartz, bassanite, apatite, fluorapatite, florencite, and rhabdophane. Compared with world hard coals, vanadium is significantly enriched with a concentration coefficient (CC) higher than 10; Mo and Pb are enriched (5 < CC < 10); F, Co, Ni, Cu, Ge, Se, Y, Zr, Nb, Ag, Cd, In, Sn, Cs, Sm, Eu, Tb, Dy, Er, Yb, Hf, Bi, and U are slightly enriched (2 < CC < 5) in the Xingying coals. Fluorine in host rocks, including roof, floor, and parting, is significantly enriched. Fluorine concentration in the coal may be increased greatly if the coal is mixed with host rocks during mining activity. Hence, the Xingying coals should be subjected to beneficiation before utilization for the environment and human health. The Al_2O_3/TiO_2 and Eu anomalies demonstrated that the terrigenous materials come from the mafic basalts of the Kangdian Upland. NH_4-illite is formed by interaction of pre-existing kaolinite or K-illite with NH_4^+ released from organic matter under high temperatures during the process of hydrothermal alteration. The authigenic chamosite, albite, quartz, anatase, apatite, fluorapatite, and rhabdophane are also deposited from the hydrothermal solutions. In addition, the Xingying coals are subjected to marine influences. Based on the preliminary evaluation, the Xingying coals cannot be a potential source for critical elements such as rare earth elements and yttrium. This indicates that not all the late Permian coals in southwestern China have economic significance for critical elements.

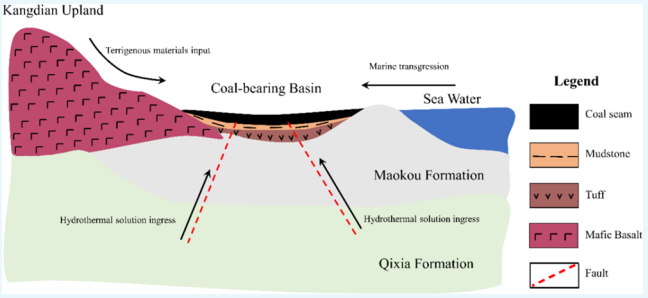

1. INTRODUCTION

In addition to organic matter, mineral matter is the other component of coal. Mineral matter encompasses crystalline minerals, noncrystalline minerals, and nonmineral elements.[1−4] Coal or coal-bearing strata are enriched significantly in critical elements such as rare earth elements and yttrium (REY), Li, Nb, Ta, Zr, Hf, Ga, Ge, etc. and have the potential to recover these critical elements.[5−11] Although organic matter is a main carrier for some critical elements (e.g., Ge) in the coal,[12,13] critical elements mainly occur in minerals.[2,4,14] Meanwhile, minerals are also main carriers for some environmentally sensitive elements, e.g., F, As, and Hg.[15−17] Moreover, modes of occurrence of minerals could provide useful information on the coal-forming process and even the regional geological background or evolution.[15,18]

Ammonian illite (NH_4-illite), with a similar structure with tobelite, is uncommon in coal.[1] However, it has been identified in some high-rank coals, varying from low volatile bituminous coal to semianthracite.[19−23] NH_4-illite is considered as an interaction product of pre-existing kaolinite or K-illite with NH_4^+ originated from organic matter decomposition during hydrothermal solution influx.[1] Thus, the presence of NH_4-illite indicates a hydrothermal alteration origin.

The late Permian coals in southwestern China (including Yunnan, Guizhou, Sichuan Provinces, and Chongqing Municipality) have intrigued scientists for more than three decades, due to their geochemical and mineralogical anomalies. The Kangdian Upland, mainly composed of mafic basalts, provided the dominant terrigenous materials for the late Permian coals in southwestern China.[24] Moreover, other geological factors, e.g., hydrothermal fluid injection, volcanic

Received: April 3, 2022
Accepted: May 18, 2022
Published: May 26, 2022

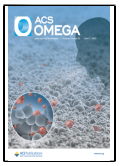

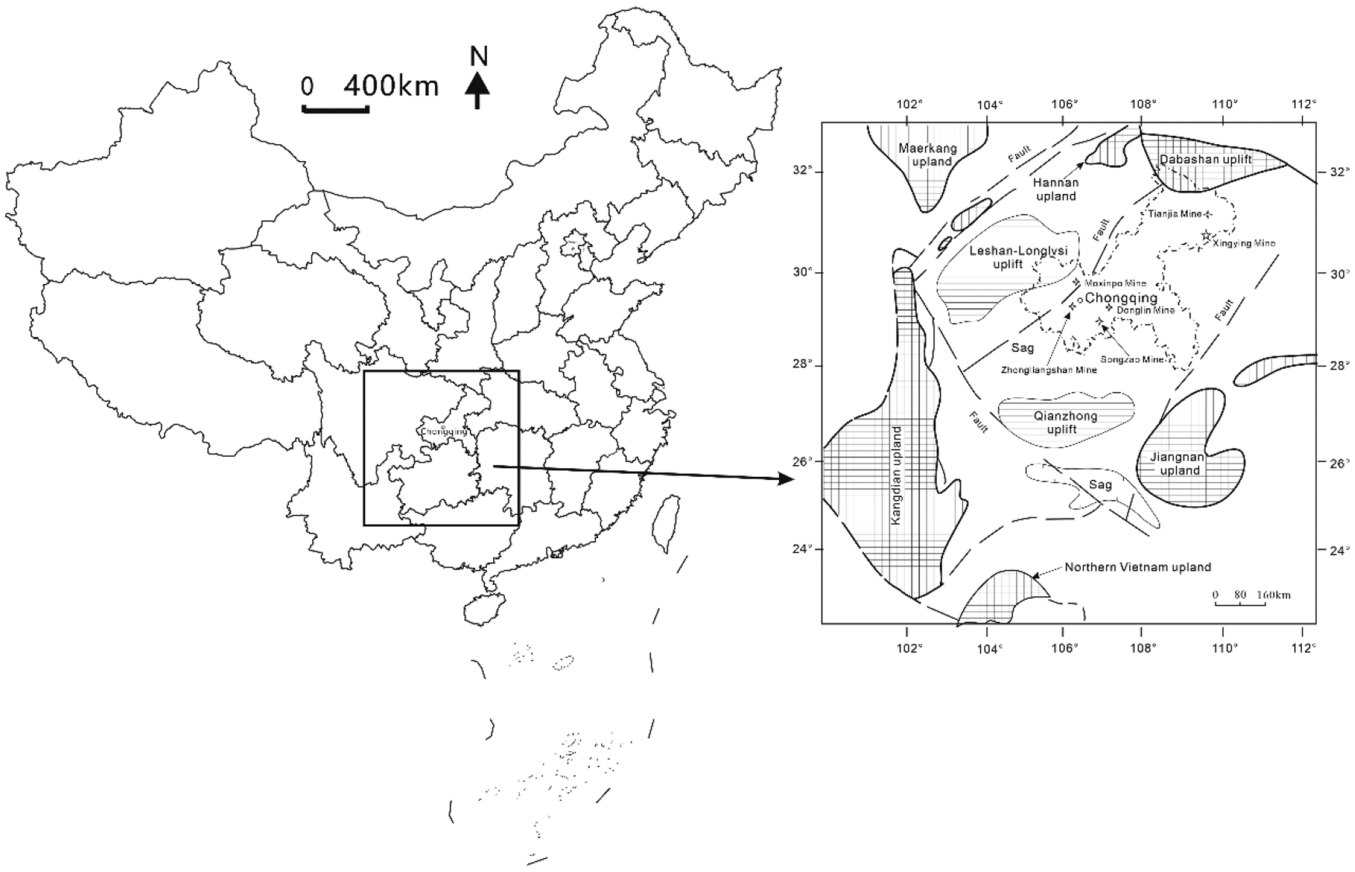

Figure 1. Location of the Xingying Mine.

ash input, and marine influences, made significant contributions to the enrichment of trace elements.[15] Anomalous critical elements, especially REY, Li, Nb, Ta, Zr, Hf, and Ga, were discovered in a few late Permian coal deposits, including Moxinpo,[23,25,26] Zhongliangshan,[27] and Songzao[28] in Chongqing, southwestern China.

The Xingying Mine, located in northeastern Chongqing, which is adjacent to the Moxinpo, Zhongliangshan, and Songzao Mines, is an important coal base for power generation (Figure 1). However, whether the late Permian coals in the Xingying Mine contain such critical elements is unclear. In addition, there is lack of mineralogical and geochemical data to discriminate the origin of terreginous materials. The purpose of this paper is to study the geochemical and mineralogical compositions, especially significantly enriched NH_4-illite, of the Xingying coals and to understand the geological factors of their formation. It also makes an preliminary evaluation of critical elements of the Xingying coals.

2. GEOLOGICAL SETTING

The coal-accumulating basin in southwestern China is located in the western Yangtze Plate (Figure 1). From west to east, the late Permian coal-bearing sequences in southwestern China vary from terristrial to transitional to marine environments.[24] During the middle Permian period, the Dongwu Movement leads to the Yangtze Plate uplift and differential erosion of the Maokou Formation. Hence, the formation of residual plains provides favorable terrian conditions for depositon of coal-bearing sequences. The Maokou Formaiton disconformably underlies with the coal-bearing sequences, which is an important sedimentary interface. Subsequently, Emeishan basalts erupt on the eroded surface of the Maokou Formation. The continuous eruption of basalts accumulates and produces the wellknown Kangdian Upland (Figure 1).

The coal-bearing stratum in the present study is the late Permian Wujiaping Formation (P_3w) with a thickness from 60.9 to 143 m (Figure 2A). The Wujiaping Formation consists of mudstone, carbonaceous mudstone, tuff layer, marl, limestone, cherty limestone, and coal seam, which is numbered as K2. The K2 is the exclusive minable coal seam in the Xingying Mine and has a thickness varying from 0.52 to 2.52 m, with an average of 1.57 m.

The Changxing Formation (P_3c) conformably overlies the Wujiaping Formation and is made up of limestone, cherty limestone, silty limestone, and limstone with banded chert. It has a thickness from 60.9 to 143 m.

The middle Permian Maokou Formation (P_2m) underlies the Wujiaping Formation inconformably. It is composed of thick-layered bioclastic limestone, cherty limestone, and limestone, with a thickness from 95.1 to 161 m.

3. SAMPLES AND ANALYTICAL PROCEDURES

The studied samples, including one roof, one parting, one roof, and eight coal samples, were collected at the Xingying underground Mine in the northeastern Chongqing Coalfield, southwestern China (Figure 2B). In order to discriminate the noncoal samples, suffixes of r, p, and f were added in the sample number to represent roof, parting, and floor samples, respectively. All the samples were preserved in plastic bags in case of pollution and oxidation.

The blocked samples were prepared to make the polished sections for vitrinite reflectance and scanning electron

https://doi.org/10.1021/acsomega.2c02062
ACS Omega 2022, 7, 18969−18984

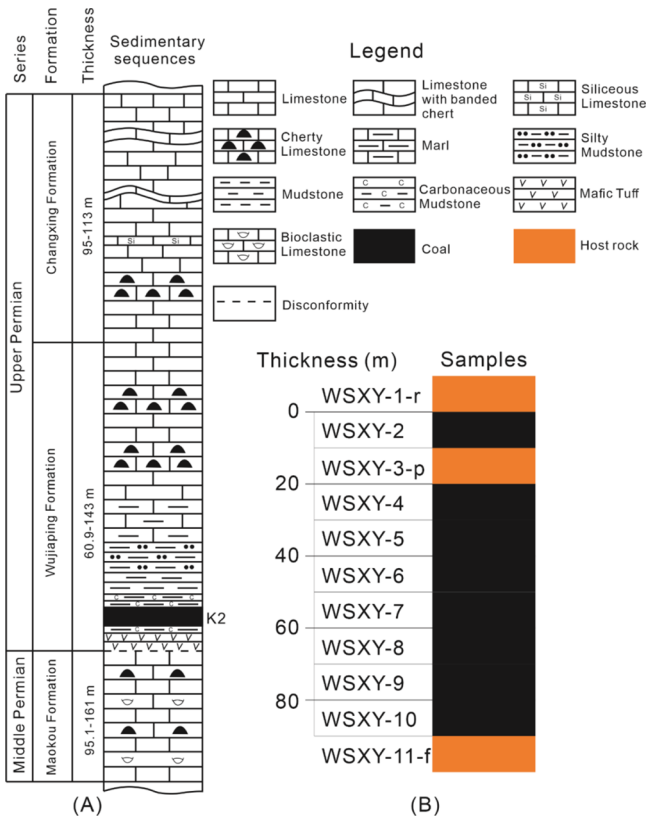

Figure 2. (A) Sedimentary sequences and the (B) collected samples of the Xingying Mine.

microscope analysis. Then, the individual samples were crushed and ground to <1 mm. Parts of <1 mm samples were further gound to <0.076 mm (200 mesh) for proximate, ultimate, mineralogical, and geochemical analyses.

The moisture, ash yield, and volatile matter were tested based on the ASTM standards D3173-11, D3174-11, and D3175-11, respectively.[29−31] The total sulfur and forms of sulfur were analyzed according to ASTM standards D3177-02 and D2492-02, respectively.[32,33] The ultimate analyses including carbon, hydrogen, and nitrogen were conducted using an element analyzer. The vitrinite random reflectances of coal polished samples were measured using a spectrophotometer equipped on an optical microscope at a magnification of 500× in which the test standard is gadolinium gallium garnet with reflectance 1.72% made in China.

Prior to X-ray diffraction (XRD), coal samples were ashed at a temperature lower than 120 °C. Then, the coal low-temperature ashes (LTAs) and roof, parting, and floor samples were subjected to mineral composition analysis. The analysis condition of XRD was reported in detail in previous studies.[23,34] Based on the XRD diffractograms, the minerals were quantitatively determined using the Siroquant technique. Five representative samples were analyzed for modes of occurrence of minerals using scanning electron microscopy in conjunction with energy-dispersive spectrometry (SEM-EDS). The SEM-EDS analysis procedure and conditions were also reported by Zou et al.[34]

The major element oxides including SiO_2, TiO_2, Al_2O_3, Fe_2O_3, MnO, MgO, CaO, Na_2O, K_2O, and P_2O_5 were determined by X-ray fluorescence (XRF) spectrometry. Prior to XRF analysis, all the coal and host rock samples were ashed at 815 °C and the resultant ashes were made into tableting samples with lithium borate.

Except for F and Hg, the trace elements were analyzed using inductively coupled plasma mass spectrometry (ICP-MS). Dai et al. described the ICP-MS analysis procedures in detail.[23] In order to avoid the interference of polyatomic ions, the collision/reaction cell technology was employed to test the concentrations of As and Se.[35]

Fluorine in the samples was tested using the pyrohydrolysis ion-selective electrode method in accordance with the ASTM D5987-96.[36] Mercury was determined using a Milestone DMA-80 analyzer with a detection limit of 0.005 ng.

4. RESULTS

4.1. Coal Characteristics. The coal quality data, including proximate and ultimate analyses, total sulfur, forms of sulfur, and vitrinite random reflectance, are listed in Table 1. The average values of volatile matter and vitrinite random reflectance are 9.15 and 3.67%, respectively, indicating a semianthracite based on the ASTM D388-12,[37] due to the plutonic metamorphism.[38] The Xingying coals have low ash yields (16.86%) and medium sulfur contents (1.66%) according to classifications of the Chinese standards GB/T 15224.1-2010 (coals with ash yields varying from 10 to 20% are low ash coals)[39] and GB/T 15224.2-2010 (coals with sulfur contents varying from 1.01 to 2% are medium sulfur coals).[40] Organic sulfur is the dominant form of total sulfur, followed by

Table 1. Proximate and Ultimate Analyses, Forms of Sulfur, and Random Vitrinite Reflectance for Coals from the Xingying Mine (%)[a]

	proximate analyses			ultimate analyses				forms of sulfur			
samples	M_{ad}	A_d	V_{daf}	C_{daf}	H_{daf}	N_{daf}	$S_{t,d}$	$S_{p,d}$	$S_{s,d}$	$S_{o,d}$	$R_{o,ran}$
WSXY-2	3.68	37.75	11.23	88.44	2.79	1.41	1.61	0.50	0.48	0.63	3.86
WSXY-4	3.48	11.61	10.46	87.95	2.62	1.50	1.55	0.28	0.69	0.58	3.73
WSXY-5	4.17	16.29	9.21	90.01	2.58	1.62	1.95	0.58	0.62	0.75	3.64
WSXY-6	5.01	15.17	6.56	91.55	2.42	1.65	1.33	0.44	0.15	0.74	3.68
WSXY-7	3.85	12.52	7.13	91.73	2.44	1.54	1.32	0.35	0.29	0.68	3.70
WSXY-8	4.71	11.65	11.71	87.42	2.52	1.40	2.98	0.51	1.31	1.16	3.47
WSXY-9	3.84	16.92	8.78	90.91	2.55	1.57	1.37	0.52	0.47	0.38	3.59
WSXY-10	3.04	12.98	8.10	90.87	2.54	1.49	1.16	0.41	0.38	0.38	3.70
average	3.97	16.86	9.15	89.86	2.56	1.52	1.66	0.45	0.55	0.66	3.67

[a]M, moisture; A, ash yield; V, volatile matter; C, carbon; H, hydrogen; N, nitrogen; S_t, total sulfur; S_p, pyritic sulfur; S_s, sulfate sulfur; S_o, organic sulfur; ad, air-dried basis; d, dry basis; daf, dry and ash-free basis; $R_{o,ran}$, vitrinite random reflectance.

https://doi.org/10.1021/acsomega.2c02062
ACS Omega 2022, 7, 18969−18984

sulfate and pyritic sulfur. However, the discrepancies among organic, sulfate, and pyritic sulfur are insignificant. The average contents of carbon, hydrogen, and nitrogen are 89.86, 2.56, and 1.52%, respectively.

4.2. Minerals. *4.2.1. Mineral Compositions in Coal LTAs, Roof, Floor, and Parting Samples.* Figure 3 shows that the

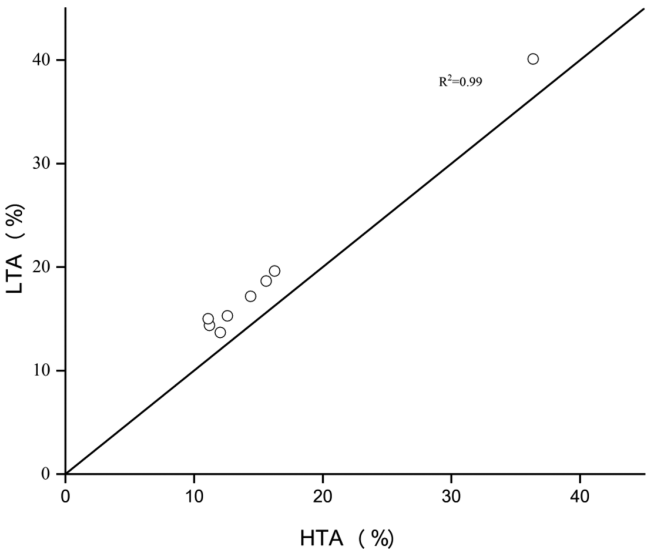

Figure 3. Comparison between high-temperature ash (HTA) and low-temperature ash (LTA).

LTAs have significant positive correlations with the high-temperature ash (HTA) yields in the Xingying coals (R^2 = 0.99). However, the LTAs are sligtly higher than the HTAs, which is not an uncommon phenomenon, confirmed by previous studies,[34,41,42] owing to the complete decomposition of minerals under high temperature conditions and the formation of new minerals under low temperature conditions. The mineralogical compositions of the Xingying coal LTAs and host rock samples are listed in Table 2. Minerals of the Xingying coal LTAs are dominated by NH_4-illite (55−74.6%) and pyrite (5.9−15.5%), followed by jarosite (1.8−23.8%), albite (1.9−32.44%), and anatase (bdl-10%) with traces of chamosite. Quartz is only present in sample WSXY-2. Bassanite is detected in samples WSXY-4 and WSXY-5. Florencite only occurs in sample WSXY-10. Minerals of the roof mainly comprise NH_4-illite, quartz, pyrite, and albite and, to a lesser extent, anatse, chamosite, and jarosite, which is similar to those of coal LTAs. However, the content of quartz in roof (13%) is much higher than that in coal LTAs. The floor and parting have similar mineral assemblages, whereas NH_4-illite is abnormally enriched (higher than 90%) with traces of anatase, chamosite, pyrite, and jarosite. In addtion, trace minerals below the XRD detection limit, such as apatite, fluorapatite, and rhabdophane, are comfirmed using SEM−EDX.

4.2.2. Ammonian Illite and Chamosite. Owing to the XRD characteristics with a d(001) crystal spacing of around 10.35 Å (Figure 4),[19,43] the illite in the Xingying coals is confirmed as ammonian illite (NH_4-illite or tobelite) rather than K-illite. NH_4-illite is considered as an interaction product between kaolinite or K-illite already present in the coal and NH_4^+ derived from decompostion of the organic matter during hydrothermal alteration at a relatively high temperature.[1,20,23] NH_4-illite is usually present in the high-rank coal seams, such as the low volatile bituminous coal of the South Walker Creek area, Australia,[20] low volatile bituminous coal of the Adaohai Mine,[19] anthracite of the Wangtaipu Mine,[21] and semi-anthracite of the Tianjia Mine,[22] China. NH_4-illite occurs as a bedding plane (Figure 5A−C) or cell-filling (Figure 5D−F). A total of 48 spots of NH_4-illite have been determined under SEM−EDX (Table 3). The content of potassium varying from the below detection limit to 3.96%, with an average of 2.54%, is lower than that of K-illite (7.5%, $K_{1.5}Al_4(Si_{6.5}Al_{1.5})O_{20}(OH)_4$).[1] Thus, the SEM-EDS data further confirmed the existence of ammonian illite. Chamosite is generally rare in coal.[44,45] However, it is not uncommon in the late Permian coals in southwestern China.[22,44,46−48] In the present study, chamosite fills in the cell cavity (Figure 6A−C), coexisting with albite or quartz. Chamosite also occurs as a colloidal form in the matrix of NH_4-illite (Figure 6D).

4.2.3. Albite and Pyrite. The Na-bearing mineral in the semianthracite of Tianjia Mine, adjacent to the Xingying Mine, is paragonite.[22] However, the Na-bearing mineral in the present study is albite. This can be confirmed not only by the XRD + Siroquant data (Table 2) but also by the SEM−EDX data (Table 3). Table 2 shows that albite is present in most coal samples, especially sample WSXY-2 with a proportion of 32.4%. The chemical compostions of albite are relatively pure and are composed of O, Al, Si, Na, and in some cases traces of Fe, with Na varying from 4.85 to 8.96% and averaging 7.38% (Table 3). In addition, the intensity of Al is approximately half that of Si in albite under EDX spectra, which is different from the paragonite EDX spectral characteristics with almost equal

Table 2. Mineralogical Compositions of Coal LTAs and Noncoal Samples by XRD and Siroquant Analysis (wt %)[a]

samples	LTA/HTA[b]	Qz	Chm	NH_4-illite	Py	Ant	Ab	Jrs	bassanite	florencite
WSXY-1-r	88.37[b]	13.0	1.7	66.3	10.1	2.7	5.7	0.6		
WSXY-2	40.1	1.1	2.2	55.0	5.9	1.6	32.4	1.8		
WSXY-3-p	84.23[b]		1.3	94.3	0.3	3.7		0.4		
WSXY-4	14.36		1.6	71.4	10.2	1.8	2.9	10.8	1.4	
WSXY-5	18.65		0.1	73.9	11.8	4.4	3.6	6.0	0.3	
WSXY-6	17.17		2.4	74.6	10.8	5.4	2.8	4.0		
WSXY-7	13.68		0.4	70.3	11.4	5.6	2.9	9.3		
WSXY-8	15			55.9	15.5		4.8	23.8		
WSXY-9	19.62		0.3	67.4	11.3	10.0	1.9	9.1		
WSXY-10	15.27		0.1	71.8	12.9	4.7	2.9	7.3		0.2
WSXY-11-f	90.43[b]		2.6	91.7	1.5	4.0		0.1		

[a]Qz, quartz; Chm, chamosite; Py, pyrite; Ant, anatase; Ab, albite; Jrs, jarosite. Blank represents below detection limits. [b]HTA.

https://doi.org/10.1021/acsomega.2c02062
ACS Omega 2022, 7, 18969−18984

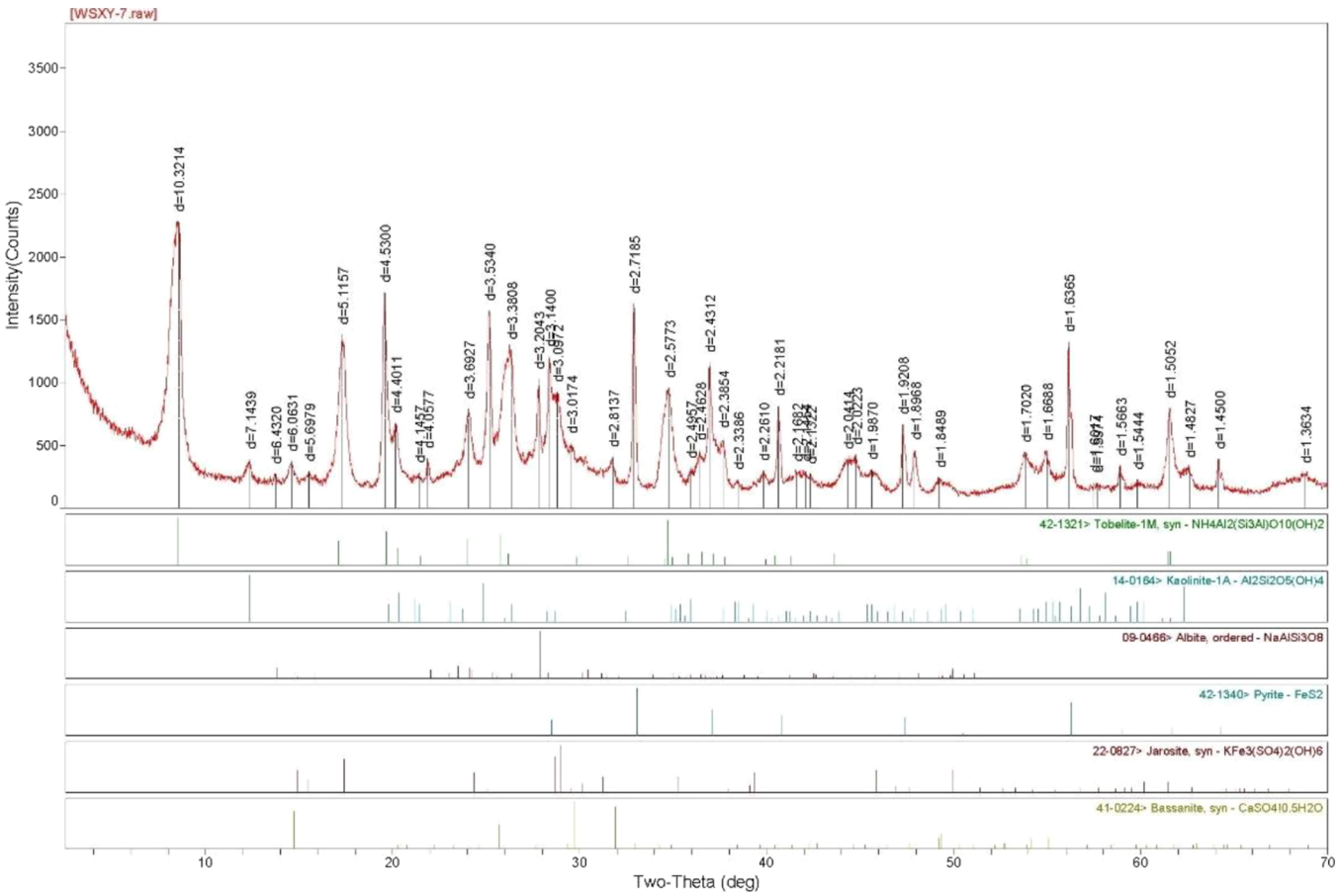

Figure 4. X-ray diffractogram of sample WSXY-7, showing ammonian illite and other phases present.

intensities of Al and Si. Albite is uncommon in the coal[4] and has been observed in the Songzao coals and Donglin coals in Chongqing.[49,50] Albite is presented in the matrix of mixed layers of illite/smectite,[49] but it occurs as cell- or fractrue-fillings (Figure 7A−D) in the present study. Pyrite is a common mineral in coals, especially in coals formed in marine environments.[51] Pyrite is relatively abundant in the Xingying coals vayring from 5.9% to 15.5% (Table 2) and occurs as a framboid and pyritohedron (Figure 8A−D).

4.2.4. Anatase and Quartz. Anatase distributes in the matrix of NH_4-illite and occurs as subhedral (Figure 9A) or colloidal form (Figure 9B). Compared to the other late Permian coals in southwestern China,[52] quartz is not enriched in the Xingying coals. Quartz fills in the cell cavity (Figure 6C) or occurs as disseminations (Figure 8A).

4.2.5. Apatite, Fluorapatite, and Rhabdophane. Apatite is observed in the roof sample and occurs as fracture-filling (Figure 7C), coexisting with albite. Fluroapatite is common in the host rocks and present as a matrix or subhedral texture (Figure 10A,B), which is the cause of the fluorine enrichement. The content of fluorine in the fluroapatite varies from 5.41 to 14.16%, with an average of 8.98% (Table 3). Rhabdophane is detected in the roof, coal, and floor samples, occurring in the granular form in the matrix of NH_4-illite (Figure 11A−F).

4.3. Geochemistry. *4.3.1. Major Elements.* The major elements in the Xingying coals are mainly composed of SiO_2, Al_2O_3, and Fe_2O_3 (Table 4). However, the contents of SiO_2, Al_2O_3, and Fe_2O_3 (7.29, 3.94, and 2.64%, respectively) in the present study are all lower than those in the Chinese coals.[15] The ratio of SiO_2/Al_2O_3 (1.78) is slightly higher than that in the Chinese coals (1.44)[15] and NH_4-illite (1.18), indicating quartz present, which is mentioned above.

4.3.2. Trace Elements. The trace element concentrations in the Xingying coals are also listed in Table 4. In order to evaluate the enrichement degree of trace elements in coal, the concentration coefficient (CC, ratio of trace element concentration in studying coals vs that in world hard coals) was proposed.[53] CC > 100, 10 < CC < 100, 10 < CC < 100, 5 < CC < 10, 2 < CC < 5, 0.5 < CC < 2, and CC < 0.5 represent unusually enriched, significantly enriched, enriched, slightly enriched, normal, and depleted, respectively.[53] Based on the classifications, vanadium is significantly enriched; Mo and Pb are enriched; F, Co, Ni, Cu, Ge, Se, Y, Zr, Nb, Ag, Cd, In, Sn, Cs, Sm, Eu, Tb, Dy, Er, Yb, Hf, Bi, and U are slightly enriched; Li, Rb, Sb, Ba, Hg, and Tl are depleted; while the remaining elements are close to the average values for world hard coals (Figure 12).

4.3.2.1. Fluorine. The concentration of fluorine in the Xingying coals varies from 228 to 589 μg/g, with an average of 378 μg/g, which is higher than the average values for Chinese coals (130 μg/g)[53] and world hard coals (82 μg/g).[54] Note that fluorine concentrations of roof, floor, and parting in the Xingying Mine are enriched significantly, where fluorine of roof, floor, and paring is up to 1889, 3385, and 2382 μg/g, respectively (Figure 13), much higher than the average values for the upper continental crust (UCC, 611 μg/g)[55] and world clay (610 μg/g).[56]

Fluorine is an environmentally sensitive element, and endemic fluorosis happened severely in western Guizhou province, where approximately 10 million people suffered from

https://doi.org/10.1021/acsomega.2c02062
ACS Omega 2022, 7, 18969−18984

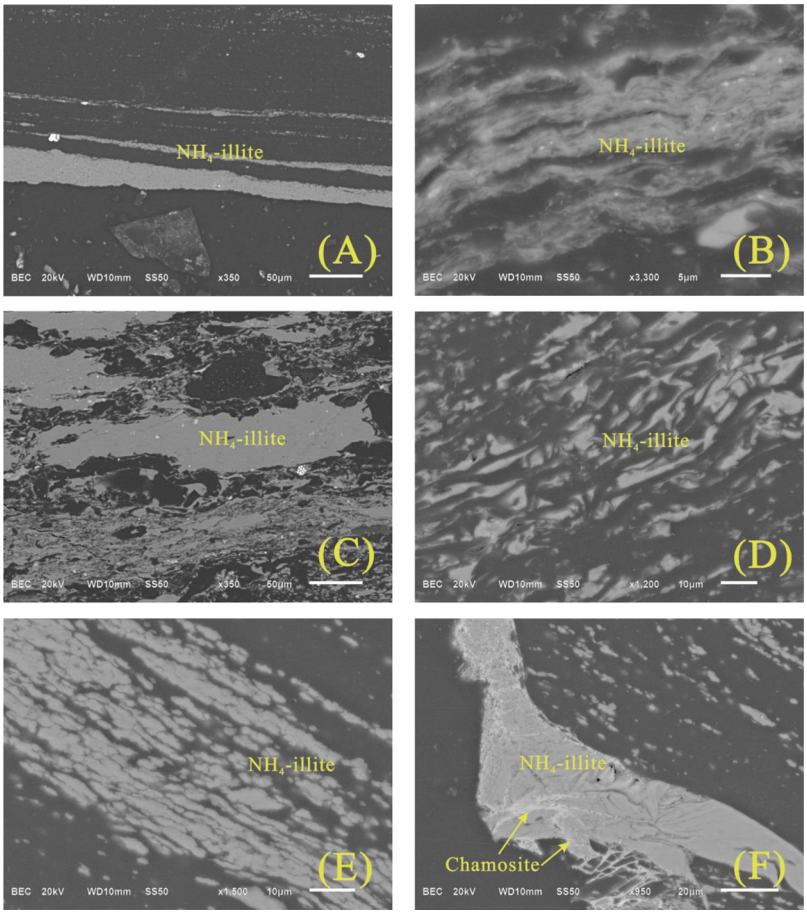

Figure 5. Modes of occurrence of NH_4-illite and other mineral phases. (A) NH_4-illite occurred as bed planes in sample WSXY-7; (B) NH_4-illite occurred as bed planes in sample WSXY-2; (C) NH_4-illite in collodetrinite in sample WSXY-7; (D) cell-filling NH_4-illite in sample WSXY-7; (E) cell-filling NH_4-illite in sample WSXY-2. (F) Fracture-filling NH_4-illite and chamosite in sample WSXY-7. Images A−F: SEM and back-scattered electron images.

dental fluorosis and 1 million people suffered from skeletal fluorosis.[57] Previous studies indicated that coal-fired fluorosis in western Guizhou province is caused by combustion of the high-F coal.[58,59] However, more and more pieces of evidence indicate that F content is within the usual range of Chinese and world coals.[57,60] Thus, it is generally considered that the endemic fluorosis is due to the combustion of high-F clay used as a briquette binder for fine coal.[15,60] The F content in the host rocks (including roof, floor, and parting) is also unusally enriched, so if the Xingying coals are mixed with these rocks when mining, the mixed coals may enrich F significantly. The local residents may suffer from endemic fluorosis if the mixed coal is burned directly without beneficiation.[61]

The correlation coefficient between F and ash yield in the Xingying coals is 0.94, indicating that F mainly occurs as mineral matter. The correlation coefficients of $r_{F\text{-}SiO2}$ and $r_{F\text{-}Al2O3}$ are 0.94 and 0.97, implying that F may associated with clay minerals. Fluorine also correlated significantly with CaO ($r_{F\text{-}CaO}$, 0.67), and the Ca-bearing minerals (e.g., fluroapatite) may be carriers of fluorine, especially in the noncoal samples (Figure 10). Fluorine is also detected in pyrite under SEM−EDX (Table 3).

4.3.2.2. Vanadium, Cr, Co, and Ni. Vanadium is enriched significantly in the Xingying coals with CC being 10.5. Cobalt (CC, 2.53) and Ni (CC, 2.97) are enriched sligtly. The content of Cr is close to the world hard coals, and the CC is 1.99. Along the coal profile, the concentration of V, Cr, Co, and Ni gradually decreases from top to botom (Figure 13).

The correlation coefficients between ash yield and V, Cr, Co, and Ni are 0.54, 0.85, 0.34, and 0.42, respectively, indicating that V and Cr have significant positive correlations with ash yield. Thus, it is inferred that V and Cr mainly occurred in the mineral matter. The correlation coefficients of V and Cr with SiO_2 ($r_{V\text{-}SiO2}$, 0.53, $r_{V\text{-}SiO2}$, 0.85) and Al_2O_3 ($r_{Cr\text{-}SiO2}$, 0.64, $r_{V\text{-}SiO2}$: 0.82) further indicate that V and Cr are associated with clay minerals. However, cobalt and Ni have both inorganic and organic affinities.

4.3.2.3. Rare Earth Elements and Yttrium (REY). The content of REY in the Xingying coals is from 82.9 to 289 μg/g and averages 131 μg/g, higher than those of the world hard coals (68 μg/g)[54] but close to those of the Chinese coals (136 μg/g).[15] Along the K2 coal profile, concentration variations of REY are insignificant except for sample WSXY-2 (Figure 13). On the basis of coal ash, only two samples (WSXY-9 and WSXY-10) have higher REY than the cutoff grade of coal ash proposed by Seredin and Dai (REO, 1000 μg/g).[11]

Based on the threefold geochemical classifications, ie., LREY, MREY, and HREY, and three enrichement types (L-type, M-type, and H-type) proposed by Seredin and Dai[11] and the upper continental crust normalization,[55] the Xingying coals are all M-REY enrichment types except for sample WSXY-7 (H-type) (Figure 14). The Xingying coals and parting all

https://doi.org/10.1021/acsomega.2c02062
ACS Omega 2022, 7, 18969−18984

Table 3. SEM−EDX Semiquantitative Analysis of Some Minerals in the Coal and Rock Samples (%; on Carbon-Free Basis)[a]

		O	F	Na	Mg	Al	Si	P	S	K	Ca	Ti	V	Fe	Cu	Mn
NH_4-illite (n = 48)	min	53.05	bdl	bdl	bdl	5.36	9.84	bdl	bdl	bdl	bdl	bdl	bdl	bdl	bdl	bdl
	max	80.40	bdl	bdl	4.01	16.50	25.72	bdl	0.77	3.96	0.98	6.31	0.46	5.97	bdl	bdl
	ave	59.88	bdl	bdl	1.80	12.62	20.81	bdl	0.06	2.54	0.03	0.65	0.01	1.63	bdl	bdl
chamosite (n = 27)	min	49.82	bdl	bdl	4.31	5.07	8.24	bdl	bdl	bdl	bdl	bdl	bdl	7.91	bdl	bdl
	max	73.43	bdl	bdl	11.23	12.89	18.62	bdl	0.60	1.78	0.50	1.61	bdl	18.27	bdl	bdl
	ave	56.54	bdl	bdl	7.25	9.41	12.81	bdl	0.05	0.25	0.03	0.15	bdl	13.51	bdl	bdl
albite (n = 13)	min	46.27	bdl	4.85	bdl	7.39	22.56	bdl	bdl	bdl	bdl	bdl	bdl	bdl	bdl	bdl
	max	62.24	bdl	8.96	bdl	13.43	33.72	bdl	bdl	bdl	bdl	bdl	bdl	1.59	bdl	bdl
	ave	55.12	bdl	7.38	bdl	9.08	28.21	bdl	bdl	bdl	bdl	bdl	bdl	0.21	bdl	bdl
pyrite (n = 20)	min	bdl	bdl	bdl	bdl	bdl	bdl	bdl	5.19	bdl	bdl	bdl	bdl	8.51	bdl	bdl
	max	66.04	7.05	bdl	4.75	10.25	15.47	2.48	57.91	2.11	5.98	1.25	bdl	45.59	3.16	0.62
	ave	26.58	0.35	bdl	0.50	2.62	3.88	0.12	34.64	0.39	0.30	0.06	bdl	30.23	0.30	0.03
anatase (n = 9)	min	50.18	bdl	bdl	bdl	0.57	1.02	bdl	bdl	bdl	bdl	12.23	bdl	bdl	bdl	bdl
	max	60.26	bdl	bdl	3.20	9.57	14.45	bdl	bdl	2.08	bdl	46.57	bdl	4.58	bdl	bdl
	ave	54.57	bdl	bdl	1.02	4.28	7.07	bdl	bdl	0.79	bdl	30.75	bdl	1.53	bdl	bdl
quartz (n = 10)	min	48.88	bdl	bdl	bdl	bdl	34.41	bdl	bdl	bdl	bdl	bdl	bdl	bdl	bdl	bdl
	max	62.85	bdl	bdl	2.07	4.05	43.04	bdl	0.62	0.85	2.74	bdl	bdl	3.29	bdl	bdl
	ave	58.15	bdl	bdl	0.37	1.27	39.38	bdl	0.06	0.16	0.27	bdl	bdl	0.33	bdl	bdl
apatite (n = 3)	min	47.03	bdl	bdl	1.36	1.34	1.94	5.32	bdl	bdl	11.92	bdl	bdl	2.89	bdl	bdl
	max	53.67	bdl	bdl	5.28	5.51	8.70	13.19	bdl	bdl	27.83	bdl	bdl	9.60	bdl	bdl
	ave	50.72	bdl	bdl	3.54	3.56	5.67	9.72	bdl	bdl	20.37	bdl	bdl	6.43	bdl	bdl
fluroapatite (n = 3)	min	43.72	5.41	bdl	bdl	bdl	bdl	13.66	bdl	bdl	28.29	bdl	bdl	bdl	bdl	bdl
	max	46.95	14.16	bdl	bdl	1.67	3.04	15.26	bdl	0.47	31.83	bdl	bdl	bdl	bdl	bdl
	ave	45.40	8.98	bdl	bdl	0.56	1.01	14.25	bdl	0.16	29.64	bdl	bdl	bdl	bdl	bdl

[a]bdl, below detection limit.

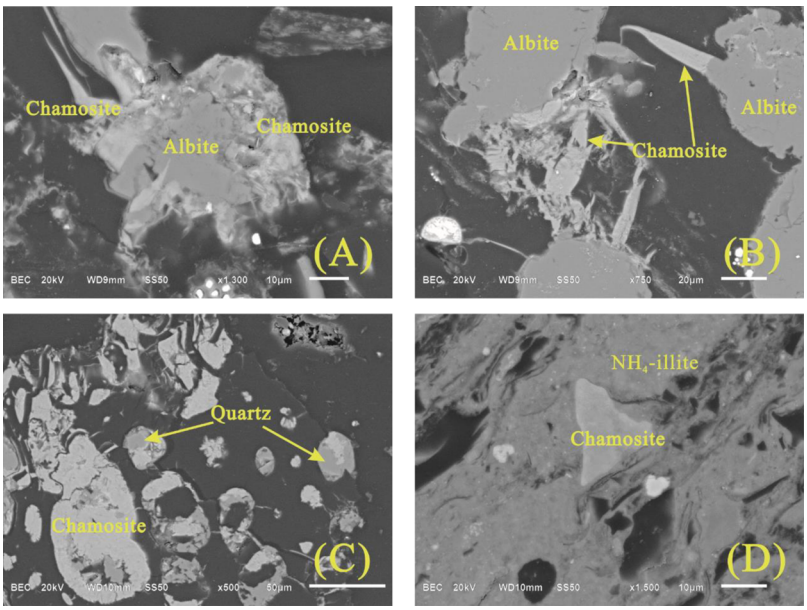

Figure 6. Modes of occurrence of chamosite and other mineral phases. (A) Cell-filling chamosite and albite in sample WSXY-2; (B) cell-filling chamosite and albite in sample WSXY-2; (C) cell-filling chamosite and quartz in sample WSXY-2. (D) Colloidal chamosite in sample WSXY-3-p. Images A−D: SEM and back-scattered electron images.

exhibit slightly Ce_N/Ce_N^* negative anomalies; however, the roof and floor show a slightly Ce_N/Ce_N^* positive anomalies. Eu_N/Eu_N^* positive anomalies occur in all the coal and host rock (including roof, floor, and parting) samples. Some studies considered that Eu may be interfered by Ba in ICP-MS when Ba/Eu is higher than 1000.[62,63] The Ba/Eu ratio of the Xingying coal and host rock samples varies from 20.2 to 130, much lower than 1000, indicating that Eu is free of Ba interference. REY in the Xingying coals correlated significantly with ash yield, with a correlation coefficient of 0.99, indicating that REY mainly occur in the inorganic matter.

5. DISCUSSION

5.1. Source of Terrigenous Materials. Kangdian Upland, derived from the Emeishan mantle plume,[50,64−66] is mainly composed of flood basalts and considered as the dominant source region providing terrigenous materials for late Permian coals in southwestern China.[42,67−69] For most late Permian coals in southwestern China, the clastic materials are the

https://doi.org/10.1021/acsomega.2c02062
ACS Omega 2022, 7, 18969−18984

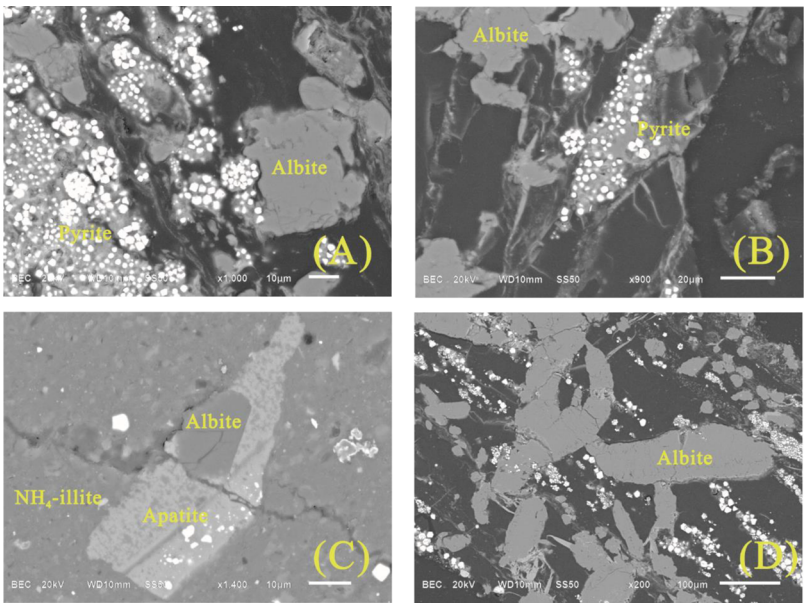

Figure 7. Modes of occurrence of albite and other mineral phases. (A) Cell-filling albite and euhedral pyrite in sample WSXY-2; (B) cell-filling albite in sample WSXY-2; (C) fracture-filling albite and apatite in sample WSXY-1-r; (D) fracture-filling albite in sample WSXY-2. Images A–D: SEM and back-scattered electron images.

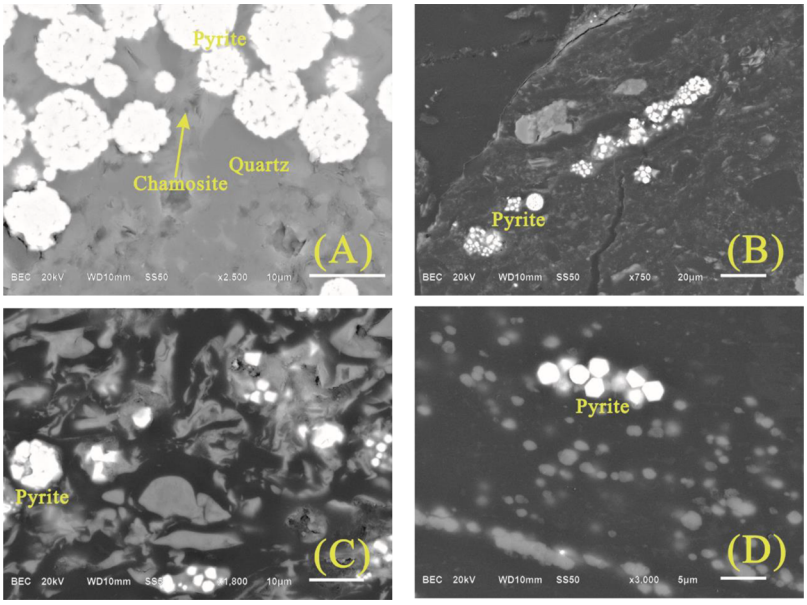

Figure 8. SEM backscattered images of pyrite and other mineral phases. (A) Framboidal pyrite and disseminated quartz in sample WSXY-1-r; (B) framboidal pyrite in sample WSXY-2; (C) cell-filling pyrite in sample WSXY-3-p; (D) pyritohedron pyrite in sample WSXY-7.

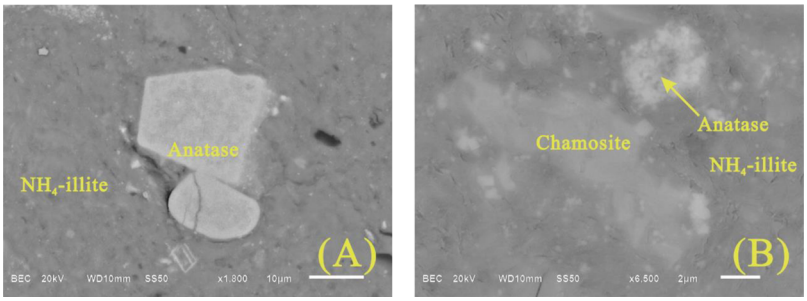

Figure 9. SEM backscattered images of anatase and other mineral phases. (A) Subhedral anatase in sample WSXY-3-p; (B) colloidal anatase in sample WSXY-11-f.

https://doi.org/10.1021/acsomega.2c02062
ACS Omega 2022, 7, 18969–18984

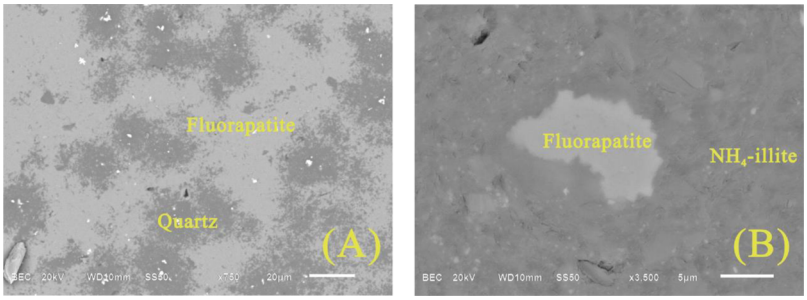

Figure 10. SEM backscattered images of fluorapatite and other mineral phases. (A) Fluorapatite and quartz in sample WSXY-1-r; (B) fluorapatite in sample WSXY-11-f.

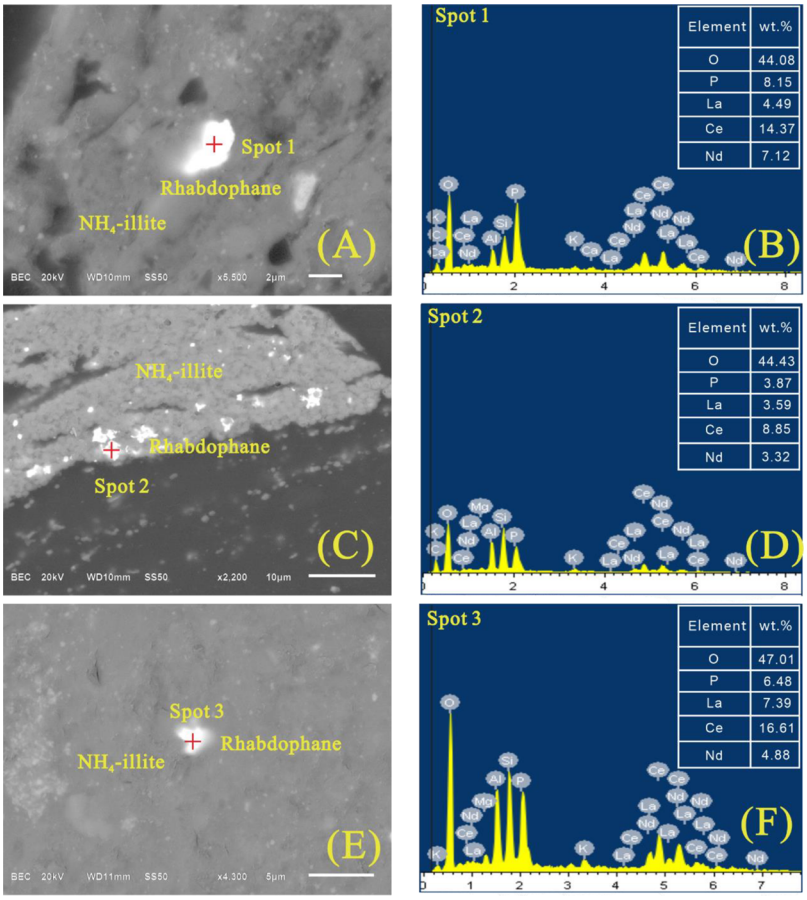

Figure 11. SEM back-scattered images and EDX spectra of rhabdophane and other mineral phases. (A) Rhabdophane occurred in the matrix of NH_4-illite in sample WSXY-3-p; (B) EDX spectrum of spot 1; (C) rhabdophane occurred in the matrix of NH_4-illite in sample WSXY-7; (D) EDX spectrum of spot 2; (E) rhabdophane occurred in the matrix of NH_4-illite in sample WSXY-11-f; (F) EDX spectrum of spot 3.

tholeiitic basalt of the Kangdian Upland.[24] However, some studies have shown that the clastic materials of late Permian coals in southwestern China are the felsic-intermediate rocks at the top of the Kangdian Upland[70] or mafic tuff[23] or other provenances.[41,50,71] The Al_2O_3/TiO_2 ratio is a reliable geochemical index for sediment source discrimination of sedimentary rocks including coal deposits,[9,72,73] which has been extensively used. The Al_2O_3/TiO_2 ratio of 3−8, 8−21, 21−70 indicates that the parent rock composition is mafic, intermediate, and felsic igneous rocks, respectively.

All the Xingying coal and host rock samples fall into the category of mafic rocks except sample WSXY-8 (Figure 15), implying that the terrigenous materials come from the mafic basalts of the Kangdian Upland. Moreover, the Eu anomaly is another parameter for indicative of the sediment source region of coal deposits.[62] If the UCC-normalized Eu anomaly occurs positive or negative in coals, it is suggested that the inorganic materials derived from mafic or felsic compositions, respectively.[62] The Eu anomaly has been used in the Huayingshan,[71] Nantong,[50] and southeastern Chongqing Coalfields[34] for indicative of the sediment source region being not the mafic basalts of the Kangdian Upland. The REY distribution patterns indicate that the inorganic material of the Xingying coals is from the mafic basalts of the Kangdian Upland, owing to the significant positive Eu anomalies, which further confirmed the results mentioned above.

5.2. Injection of Hydrothermal Fluids. Injection of hydrothermal fluids plays an important role in the enrichment

https://doi.org/10.1021/acsomega.2c02062
ACS Omega 2022, 7, 18969−18984

Table 4. Loss on Ignition (LOI, %), Percentages of Major Element Oxides (%), and Concentrations of Trace Elements (μg/g) for Coal and Host Rock Samples in the Xingying Mine (on Coal or Rock Basis)[a]

	WSXY-													
element	1-r	2	3-p	4	5	6	7	8	9	10	11-f	avg	world coal[57]	CC
LOI	11.63	63.64	15.77	88.80	84.39	85.59	87.96	88.90	83.73	87.41	9.57	83.8	nd	
SiO_2	48.36	18.68	44.59	4.66	6.68	6.34	5.38	4.16	6.73	5.71	48.42	7.29	8.47[b]	
TiO_2	2.3	1.3	4.23	0.43	1.15	1.2	0.77	0.11	1.9	0.75	4.54	0.95	0.33[b]	
Al_2O_3	17.82	8.43	22.18	2.73	3.86	3.74	3.12	2.33	3.98	3.35	23.66	3.94	5.98[b]	
Fe_2O_3	9.72	4.29	5.17	2.48	2.72	1.99	1.72	3.72	2.45	1.73	4.02	2.64	4.85[b]	
MnO	0.051	0.006	0.022	0.003	0.002	0.002	0.003	0.002	0.003	0.002	0.008	0	0.02[b]	
MgO	4.29	1.44	2.99	0.25	0.34	0.32	0.29	0.25	0.34	0.29	4.18	0.44	0.22[b]	
CaO	0.79	0.14	0.31	0.14	0.15	0.17	0.17	0.08	0.16	0.17	0.4	0.15	1.23[b]	
Na_2O	0.384	0.527	0	0.011	0.03	0.021	0.022	0.015	0.014	0.021	0	0.08	0.16[b]	
K_2O	3.44	1.03	3.82	0.29	0.41	0.37	0.31	0.29	0.41	0.33	4.49	0.43	0.19[b]	
P_2O_5	0.344	0.029	0.048	0.009	0.014	0.015	0.011	0.008	0.018	0.012	0.039	0.01	0.09[b]	
Al_2O_3/SiO_2	2.71	2.22	2.01	1.71	1.73	1.7	1.72	1.79	1.69	1.7	2.05	1.78	1.42[b]	
Li	27.4	9.45	16.9	2.08	2.99	1.56	2.14	1.95	2.04	1.52	16.6	2.97	12	0.25
Be	5.83	1.78	5.64	1.78	2.29	2.36	2.48	1.2	2.37	2.32	2.5	2.07	1.6	1.30
B	193	88.2	309	51.2	66.6	68.1	55.8	37.8	65.4	57	350	61.2	52	1.18
F	1889	551	2382	265	393	390	589	228	327	278	3385	378	88	4.29
Sc	12.5	11.8	26.5	3.15	6.44	5.97	4.69	2.44	6.89	4.76	19.8	5.77	3.9	1.48
V	156	412	482	310	364	316	155	107	243	186	641	262	25	10.46
Cr	153	36.2	191	22.9	42.8	38.1	26.9	19.7	40.8	27.1	73.2	31.8	16	1.99
Co	26.4	13.5	21.1	9.88	15.1	14.7	14.7	6.9	13.7	14.6	4.66	12.9	5.1	2.53
Ni	71.3	30.6	53.1	43.7	55.2	49.3	36.8	16.1	39.9	37	34.4	38.6	13	2.97
Cu	142	96.2	211	44.1	93.9	77.2	48.4	27.9	123	63.8	130	71.7	16	4.48
Zn	183	35.1	117	23.6	40.2	27.5	26.8	25.4	27.6	22	37.4	28.5	23	1.24
Ga	27.6	12	40.6	8.48	10.9	11.5	10.1	6.99	9.99	9.2	38.1	9.88	5.8	1.70
Ge	2.24	1.64	5.43	4.63	5.7	5.77	5.84	3.26	4.3	4.23	4.11	4.42	2.2	2.01
As	4.64	2.45	3.79	6.07	6.68	4.39	4.3	8.27	6.39	4.52	1.1	5.38	8.3	0.65
Se	3.01	5.08	9.03	4.82	4.83	3.93	4.14	4.64	5.97	4.78	1.31	4.77	1.3	3.67
Rb	50.8	14.5	70.7	4.76	6.63	5.73	4.52	5.27	6.73	4.75	93.3	6.61	14	0.47
Sr	426	161	435	132	146	157	161	101	154	152	424	145	110	1.32
Y	41.8	39	52.3	22.5	26.3	27.9	24.9	25.7	31.1	28.9	22	28.3	8.4	3.37
Zr	580	379	627	56.2	121	111	76.3	42.3	122	82.5	618	124	36	3.44
Nb	70.1	10.3	108	3.53	9.63	8.12	7.36	3.38	19.2	10.1	87.3	8.96	3.7	2.42
Mo	1.51	2.74	5.3	14.3	22.9	22.5	20.2	11	15.9	15.6	11.1	15.64	2.2	7.11
Ag	2.17	1.23	2.36	0.19	0.53	0.38	0.26	0.16	0.44	0.28	2.23	0.44	0.095	4.58
Cd	1.85	0.79	2.19	0.38	0.50	0.44	0.39	0.46	0.42	0.37	0.83	0.47	0.22	2.13
In	0.2	0.12	0.2	0.05	0.11	0.1	0.07	0.04	0.13	0.08	0.27	0.09	0.031	2.83
Sn	5.47	2.73	4.93	1.59	3.34	3.44	3.14	1.44	3.06	2.45	5.51	2.65	1.1	2.41
Sb	0.12	0.08	0.53	0.09	0.42	0.37	0.33	0.23	0.31	0.32	0.11	0.27	0.92	0.29
Cs	15.2	2.14	15.3	bdl	bdl	bdl	bdl	bdl	bdl	bdl	13.1	2.14	1	2.14
Ba	115	47.9	197	29.9	45.5	46.5	33.9	18.9	49.2	34.9	207	38.3	150	0.26
La	58.5	50.1	75.1	9.41	17.2	14.9	10.1	8.83	19.8	12.2	18.9	17.8	11	1.62
Ce	133	93.8	149	19.1	32	29.8	20.8	18.6	42.5	26.4	40.1	35.4	23	1.54
Pr	14.8	12.6	16.9	2.75	4.32	4.1	2.97	2.8	5.96	3.81	4.26	4.91	3.5	1.40
Nd	59.8	51.3	66.1	12.4	18.3	17.6	13.3	13	25.8	17	17.2	21.1	12	1.76
Sm	12.1	9.68	12.8	3	4.08	3.9	3.21	3.28	5.56	3.9	5.14	4.58	2	2.29
Eu	2.77	2.38	3.17	0.77	1.08	1.05	0.87	0.85	1.41	1.03	1.6	1.18	0.47	2.51
Gd	12.8	9.38	13.5	3.57	4.65	4.67	3.96	3.98	6.18	4.63	6.19	5.13	2.7	1.90
Tb	1.86	1.27	1.95	0.56	0.72	0.73	0.64	0.63	0.88	0.71	0.99	0.77	0.32	2.40
Dy	10.7	7.48	11.3	3.66	4.61	4.81	4.23	4.13	5.32	4.67	5.83	4.86	2.1	2.32
Ho	1.99	1.48	2.06	0.72	0.92	0.96	0.88	0.79	1.03	0.92	0.98	0.97	0.54	1.79
Er	5.73	4.64	5.51	2.15	2.76	2.88	2.68	2.25	2.99	2.83	2.66	2.9	0.93	3.12
Tm	0.75	0.67	0.7	0.28	0.36	0.39	0.36	0.29	0.38	0.35	0.34	0.38	0.31	1.24
Yb	5.02	4.87	4.41	1.84	2.47	2.47	2.43	1.84	2.41	2.26	2.33	2.57	1	2.57
Lu	0.7	0.71	0.59	0.25	0.34	0.35	0.35	0.26	0.33	0.32	0.31	0.36	0.2	1.81
Hf	14.5	7.45	17.3	1.56	3.11	2.9	2.05	1.22	3.11	2.24	15.2	2.96	1.2	2.46
Ta	3.15	0.49	8.16	bdl	0.34	0.23	0.23	0.06	1.24	0.47	6.25	0.44	0.28	1.56
W	1.97	0.26	3.66	0.44	0.52	0.53	0.53	0.29	1.95	0.65	3.47	0.65	1.1	0.59
Bi	0.5	0.4	0.31	0.12	0.31	0.32	0.24	0.23	0.39	0.28	0.63	0.29	0.1	2.86

https://doi.org/10.1021/acsomega.2c02062
ACS Omega 2022, 7, 18969−18984

Table 4. continued

element	WSXY-1-r	WSXY-2	WSXY-3-p	WSXY-4	WSXY-5	WSXY-6	WSXY-7	WSXY-8	WSXY-9	WSXY-10	WSXY-11-f	avg	world coal[57]	CC
Hg	0.09	0.15	0.11	0.13	0.12	0.1	0.09	0.16	0.13	0.11	0.05	0.12	0.63	0.19
Tl	0.32	0.03	0.28	0.05	0.08	0.03	0.01	0.1	0.04	0.02	0.14	0.04	7.8	0.01
Pb	17.8	5	10.4	7.64	9.43	6.74	5.69	11.8	7.93	5.77	5.15	7.5	0.97	7.73
Th	9.59	4.9	15.9	1.68	3.1	2.78	2.08	1.51	2.99	1.99	14.7	2.63	3.3	0.80
U	3.7	11.1	18.5	7.54	7.81	5.22	4.32	8.62	8.14	4.05	13.8	7.1	2.4	2.96

[a]CC, concentration coefficient, ratio between the average value of individual elements in studied coals and the mean value in world hard coals; bdl, below detection limit; nd, no data. [b]The data are cited from Dai et al.[15]

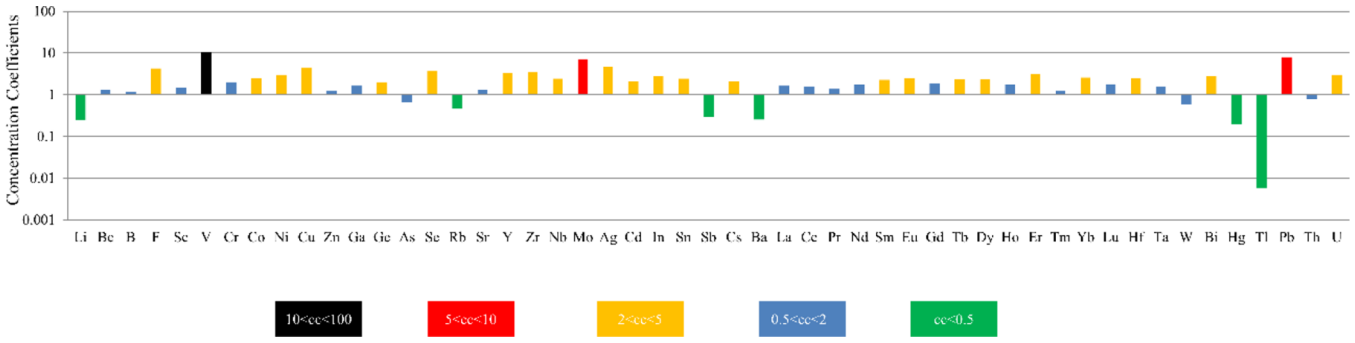

Figure 12. Concentration coefficients of trace elements in the Xingying coals.

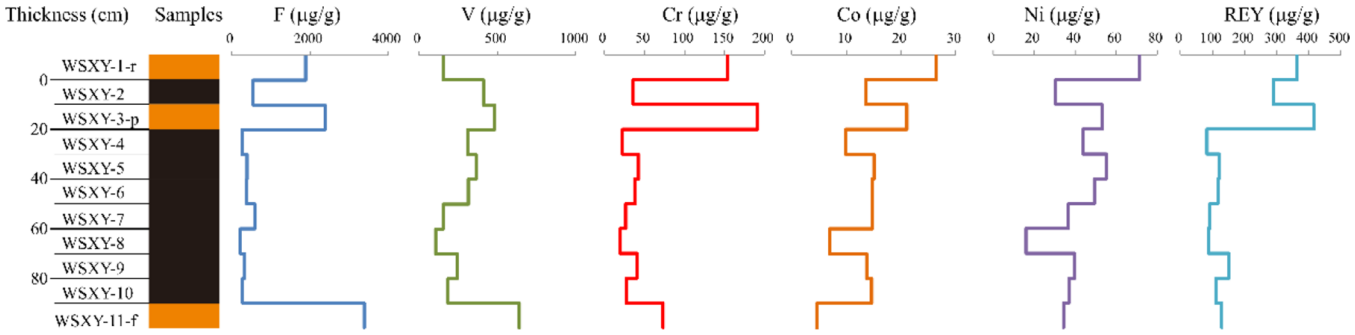

Figure 13. Variations of F, V, Cr, Co, Ni, and REY along the coal seam profile.

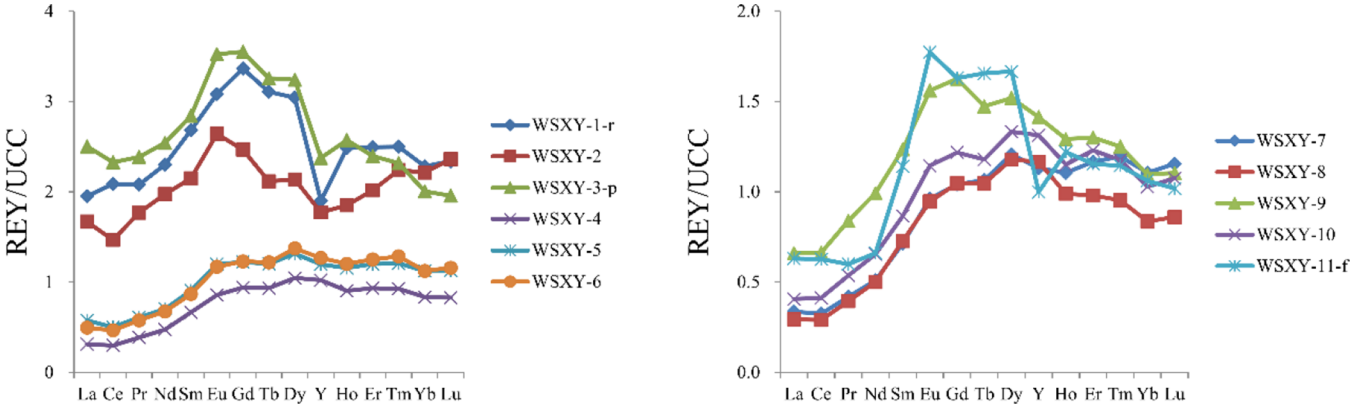

Figure 14. UCC-normalized REY distribution patterns of coal and host rock samples in the Xingying Mine. REY data of upper continental crust (UCC) are from Taylor and Mclennan.[55]

of trace elements especially the critical elements in the coal seams.[2,18,22,74] Previous studies have proved that geochemical and mineralogical anomalies of coals in southwestern China are attributed to the hydrothermal solutions.[23,75−77] Zhou et al. demonstrated that the Tianjia coals, adjacent to the present study area, were significantly affected by the hydrothermal solutions on the basis of Sr. isotope signature and mineral assemblages.[22] Similarly, the Xingying coals are also affected by the hydrothermal fluids, leading to the mineralogical and geochemical anomalies. There are some mineralogical and geochemical evidence.

https://doi.org/10.1021/acsomega.2c02062
ACS Omega 2022, 7, 18969−18984

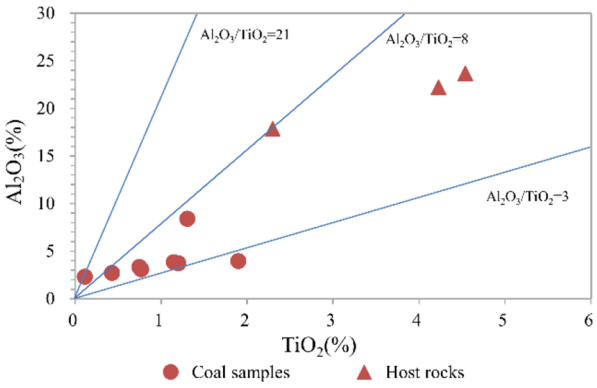

Figure 15. Relationships between Al_2O_3 and TiO_2 for coal and host rock samples in the Xingying Mine.

NH_4-illite is considered an interaction product between pre-existing kaolinite or K-illite and NH_4^+ decomposed from organic matter at a relatively high temperature during hydrothermal alteration.[20,21,23,78] Due to the high formation temperature (>250 °C),[43] NH_4-illite is usually present in the high rank coals and associated rocks.[1,19,20,78−81] Based on the nitrogen isotope discrepancy between inorganic and organic matter, Xie et al. confirmed the hydrothermal origin of NH_4-illite.[82] Thus, the presence of NH_4-illite is indicative of precipitates derived from hydrothermal fluids that passed through the coal or subjected to increased geothermal gradients.[1,22] NH_4-illite is enriched and distributed in the cell cavities or fractures (Table 3; Figure 5D−F) in the Xingying coals, providing evidence for the hydrothermal origin. During the hydrothermal alteration process, NH_4-illite is formed by interaction of pre-existing kaolinite or K-illite with NH_4^+ released from organic matter under high temperatures. Owing to the kaolinite or K-illite absence under SEM, the pre-existent kaolinite or K-illite may be completely altered by the hydrothermal solutions.

Chamosite is also a typical mineral in relation to the hydrothermal origin. It is formed by interaction of pre-existing kaolinite and Fe−Mg-rich fluids[20,44,48] or directly deposited from the siliceous solutions containing Fe−Mg.[46] In the present study, chamosite, independent of kaolinite, occurs in the cell-fillings (Figure 6A−C), indicating its hydrothermal origin. Albite of detrital origin was found in the roof sample from borehole 11,424 of Bowen Basin, Australia.[20] However, the occurrence of albite with cell- or fracture-filling (Figure 7A−D) in the present study indicates its authigenic origin. Another Na-bearing mineral, paragonite, is considered to be the result of hydrothermal alteration,[20,22] and this may also be the mechanism of albite in the present study. The cell-filling quartz was also identified (Figure 6C), indicating an authigenic origin. Additionally, chamosite, albite, and quartz occur in the same cell or fracture (Figure 6A−C), suggesting that the Xingying coals were subjected at least three injections of hydrothermal fluids.[1,22] In the hydrothermal fluid injections, the compositions of each fluid changed, leading to the formation of different minerals.[83] Based on the occurrence of these three minerals, chamosite formed earlier than quartz but later than albite.

The subhedral and colloidal anatase and fracture-filling apatite also suggest a hydrothermal origin. Rhabdophane, a secondary mineral containing REY, is rare in coal but is not uncommon in late Permian coals from southwestern China and considered as a product in relation to the hydrothermal origin.[23,34] Rhabdophane was confirmed in the roof, coal, and floor samples and occured in the granular form in the matrix of NH_4-illite (Figure 11A−F), indicating a hydrothermal origin.

Gadolinium generally shows very weak negative anomalies in Chinese and US coals.[62] However, the coals influenced by hydrothermal solutions or other waters exhibit positive or weakly positive anomalies.[62,84] The Xingying coals occur weakly Gd positive anomalies varying from 0.96 to 1.19 and averaging 1.08 (Table 5) and are characterized by M-type REY patterns (Figure 14), which are typical of acid waters, including high pCO_2-waters in coal basins.[84] Another evidence for the hydrothermal fluid injection in the present study is the redistribution of elements such as Nb/Ta, Zr/Hf, and U/Th in the coal, parting, roof, and floor samples. It is generally acknowledged that ratios of Nb/Ta, Zr/Hf, and U/Th in the coal altered by hydrothermal fluids are higher than those in the parting, roof, and floor samples.[71,77] Ratios of Nb/Ta, Zr/Hf, and U/Th in sample WSXY-2 are higher than those in the underlying parting (WSXY-3-p) (Figure 16). These element pairs in sample WSXY-10 are also higher than those in the underlying floor except for Zr/Hf (Figure 16). The geo-

Table 5. REY Geochemical Parameters of Coal and Host Rock Samples in the Xingying Mine[a]

sample no.	REY (μg/g)	La_N/Lu_N	La_N/Sm_N	Gd_N/Lu_N	enrichment type	Ce_N/Ce_N*	Eu_N/Eu_N*	Y_N/Ho_N	Gd_N/Gd_N*	La_N/La_N*
WSXY-1-r	363	0.83	0.73	1.44	M−H	1.04	1.03	0.76	1.13	1.19
WSXY-2	289	0.71	0.78	1.04	M−H	0.85	1.15	0.96	1.16	1.23
WSXY-3-p	415	1.28	0.88	1.81	L−M	0.95	1.11	0.92	1.14	1.21
WSXY-4	82.9	0.38	0.47	1.14	M−H	0.86	1.08	1.13	1.11	1.49
WSXY-5	120	0.51	0.63	1.08	M−H	0.85	1.14	1.04	1.11	1.37
WSXY-6	116	0.43	0.57	1.06	M−H	0.87	1.13	1.05	1.12	1.30
WSXY-7	91.6	0.29	0.47	0.90	H	0.86	1.12	1.02	1.10	1.42
WSXY-8	87.2	0.34	0.40	1.22	M−H	0.85	1.08	1.18	1.11	1.62
WSXY-9	152	0.60	0.53	1.47	M−H	0.89	1.10	1.09	1.17	1.24
WSXY-10	110	0.38	0.47	1.13	M−H	0.88	1.11	1.14	1.13	1.35
WSXY-11-f	129	0.62	0.55	1.60	M−H	1.02	1.30	0.82	1.10	1.32
Average	131	0.45	0.54	1.13		0.86	1.11	1.08	1.13	1.38

[a]La_N/Lu_N, ratio between La_N and Lu_N; La_N/Sm_N, ratio between La_N and Sm_N; Gd_N/Lu_N, ratio between Gd_N and Lu_N; Y_N/Ho_N, ratio between Y_N and Ho_N; $Ce_N/Ce_N^* = Ce_N/(0.5La_N + 0.5Pr_N)$; $Eu_N/Eu_N^* = Eu_N/(0.5Sm_N + 0.5Gd_N)$; $Gd_N/Gd_N^* = Gd_N/[(Sm_N \times 0.33) + (Tb_N \times 0.67)]$; $La_N/La_N^* = La_N/(3Pr_N - 2Nd_N)$; N, upper continental crust normalized; L, light rare earth element enrichment; M, medium rare earth element enrichment; H, heavy rare earth element enrichment.

https://doi.org/10.1021/acsomega.2c02062
ACS Omega 2022, 7, 18969−18984

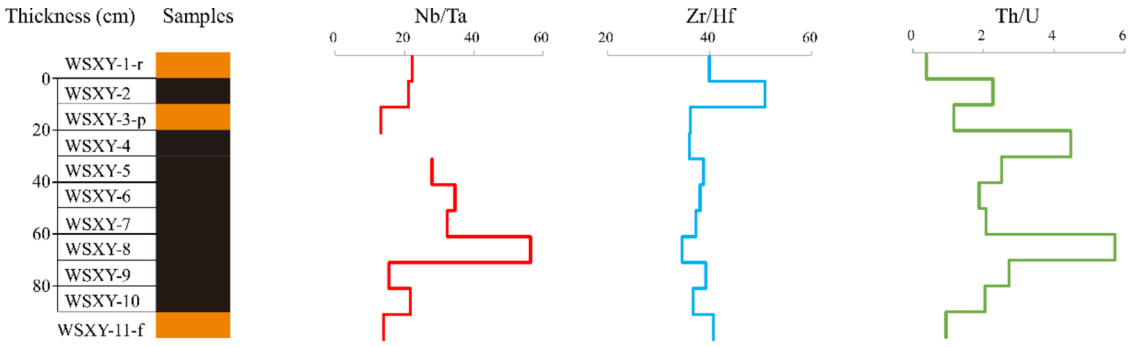

Figure 16. Variations of Nb/Ta, Zr/Hf, and U/Th along the coal seam profile.

chemical evidence further confirmed that the Xingying coals are influenced by the injection of hydrothermal fluids.

5.3. Marine Influence. Marine sediment environments also make contribution to the trace element enrichment. Being sensitive to the sedimentary environment, B/Ga and Sr/Ba ratios are usually used as indices for sedimentary environment indicatives.[85] Boron and Ga are two different elements. Borate has high solubility and could migrate over long distances. The inactive gallium, however, is easy to be precipitated during migration processes. The B/Ga ratios being <1.5, 1.5−3, and >4−5 represent fresh, brackish, and saline water facies, respectively.[86] Strontium and Ba usually combine with SO_4^{2-} to form $SrSO_4$ and $BaSO_4$, respectively. Owing to the different solubility, $BaSO_4$ could be precipitated adjacent to provenance area and $SrSO_4$ could be transported over long distances and precipitated in the ocean.[85] Hence, Sr in marine sediments has high Sr content and Sr/Ba ratios. The Sr/Ba ratios higher than 1 and lower than 1 indicate marine and continental environments, respectively.[85] The B/Ga and Sr/Ba ratios in the Xingying coals are all higher than 4 and 1, respectively, indicating that the Xingying coals are deposited in marine environments. As mentioned above, the total sulfur in the Xingying coals varies from 1.16 to 2.98% and averages 1.66%, also indicating a seawater-influenced deposition environment. Additionally, seawater is characterized by Y positive anomalies, so coals subjected to the seawater influence would expect to have positive Y anomalies.[62,85] Yttrium in the Xingying coals shows significant positive anomalies (Figure 14), further demonstrating the marine influence.

5.4. Critical Elements. Due to their irreplaceable applications in modern technologies, REY are considered as critical elements.[11,62,87] In order to meet the increasing growth of REY demand, discovering new deposits is necessary.[5,87] Fortunately, coal and coal byproducts have the potential to provide REY in the foreseeable future.[8,11,88−92] The late Permian coals in southwestern China have been reported repeatedly for enrichment of REY.[9,23,27,42,68,93] Seredin and Dai proposed the cut-off grade of oxides of REY in coal ash (1000 μg/g) and an evaluation index, outlook coefficient (C_{outl}).[11] REY with the $C_{outl} > 2.4$, $0.7 \leq C_{outl} < 1.9$, and $C_{outl} < 0.7$ represent highly promising, promising, and unpromising, respectively.[23] Based on the relationship between cut-off grade and C_{outl}, most coal benches, the roof, parting, and the floor fall within the unpromising area (Figure 17). Only two coal benches (WSXY-9 and WSXY-10) are within the promising area. However, the thickness of these two coal benches is thin (20 cm). Therefore, unlike other late Permian coals, the Xingying coals have no potential for extracting REY. The location of the present study is far away from the sediment

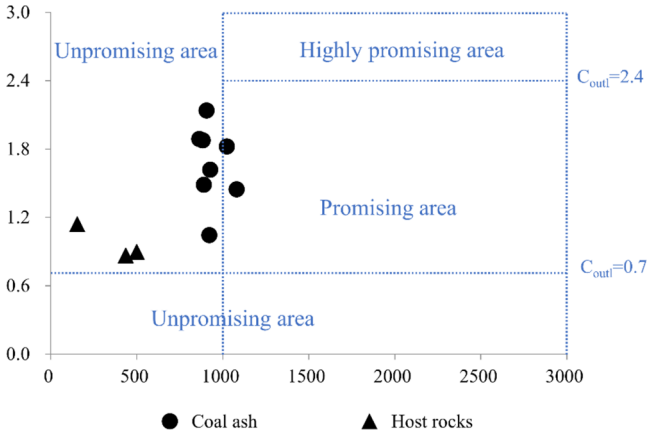

Figure 17. Evaluation of REY in the coal ashes and host rocks in the Xingying Mine.

source region, which may lead to a relatively lesser REY input. In addition, the hydrothermal fluids may contain lesser REY compositions, compared with other later Permian coals enriched with REY.

6. CONCLUSIONS

The Xingying coals are classified as semianthracite owing to the plutonic metamorphism, with low ash and medium sulfur. The sulfur in coal is dominated by organic sulfur, followed by sulfate and pyritic sulfur. NH_4-illite, which accounts for more than 50% in minerals, is significantly enriched in the Xingying coals. The other minerals include pyrite and, to a lesser extent, jarosite, albite and anatase, with traces of chamosite, quartz, bassanite, apatite, fluorapatite, florencite, and rhabdophane. NH_4-illite is formed by the interaction of pre-existed kaolinite or K-illite with NH_4^+ decomposed from organic matter at high temperatures during hydrothermal solution ingress. The hydrothermal solution ingress also resulted in deposition of chamosite, albite, quartz, anatase, apatite, fluorapatite, and rhabdophane. The Xingying coals enrich V, Mo, Pb, F, Co, Ni, Cu, Ge, Se, Y, Zr, Nb, Ag, Cd, In, Sn, Cs, Sm, Eu, Tb, Dy, Er, Yb, Hf, Bi, and U, compared with world coals. The F content in the host rocks (including roof, floor, and parting) is unusally enriched, so if the Xingying coals are mixed with these rocks when mining, the mixed coals may enrich F significantly. The local residents may suffer from endemic fluorosis if the mixed coal is burned directly without beneficiation, which requires attention. The inorganic material of the Xingying coals comes from the mafic basalts of the Kangdian upland. Additionally, marine environments also make contribution to the inorganic

https://doi.org/10.1021/acsomega.2c02062
ACS Omega 2022, 7, 18969−18984

material formation in the Xingying coals. Unlike other late Permian coals in southwestern China, the Xingying coals cannot be considered as alternative sources for extraction of REY.

AUTHOR INFORMATION

Corresponding Author

Jianhua Zou − *School of Civil Engineering, Chongqing Three Gorges University, Chongqing 404020, China; Chongqing Key Laboratory of Exogenic Mineralization and Mine Environment, Chongqing Institute of Geology and Mineral Resources, Chongqing 401120, China;* orcid.org/0000-0002-5732-1783; Email: zoujianhua@sanxiau.edu.cn

Authors

Hui Wang − *School of Civil Engineering, Chongqing Three Gorges University, Chongqing 404020, China*

Hongyu Chen − *School of Civil Engineering, Chongqing Three Gorges University, Chongqing 404020, China*

Hang Li − *School of Civil Engineering, Chongqing Three Gorges University, Chongqing 404020, China; Chongqing Key Laboratory of Exogenic Mineralization and Mine Environment, Chongqing Institute of Geology and Mineral Resources, Chongqing 401120, China*

Tian Li − *Chongqing Key Laboratory of Exogenic Mineralization and Mine Environment, Chongqing Institute of Geology and Mineral Resources, Chongqing 401120, China*

Complete contact information is available at: https://pubs.acs.org/10.1021/acsomega.2c02062

Notes

The authors declare no competing financial interest.

ACKNOWLEDGMENTS

The research was financially supported by the National Natural Science Foundation of China (41502162), Natural Science Foundation of Chongqing Municipality (cstc2020jcyj-msxmX0042), the Cooperation Program of Chongqing Municipal Education Commission and Chinese Academy Sciences (HZ2021012), and the Science and Technology Research Program of Chongqing Municipal Education Commission (KJQN202001206 and KJZD-M202101201). We thank Dr. Mingxuan Zhou at China University of Mining and Technology (Beijing) for the assistance of mineral quantification.

REFERENCES

(1) Ward, C. R. Analysis, origin and significance of mineral matter in coal: An updated review. *Int. J. Coal Geol.* **2016**, *165*, 1−27.

(2) Dai, S.; Finkelman, R. B.; French, D.; Hower, J. C.; Graham, I. T.; Zhao, F. Modes of occurrence of elements in coal: A critical evaluation. *Earth-Sci. Rev.* **2021**, *222*, No. 103815.

(3) Dai, S.; Hower, J. C.; Finkelman, R. B.; Graham, I. T.; French, D.; Ward, C. R.; Eskenazy, G.; Wei, Q.; Zhao, L. Organic associations of non-mineral elements in coal: A review. *Int. J. Coal Geol.* **2020**, *218*, No. 103347.

(4) Finkelman, R. B.; Dai, S.; French, D. The importance of minerals in coal as the hosts of chemical elements: A review. *Int. J. Coal Geol.* **2019**, *212*, No. 103251.

(5) Lin, R.; Soong, Y.; Granite, E. J. Evaluation of trace elements in U.S. coals using the USGS COALQUAL database version 3.0. Part I: Rare earth elements and yttrium (REY). *Int. J. Coal Geol.* **2018**, *192*, 1−13.

(6) Nechaev, V. P.; Dai, S.; Zhao, L.; Moore, T. A.; Nechaeva, E. V. The Tarim Basin, China, a prospect for plume-related Zr(Hf)-Nb(Ta)-REY-Ga-U mineralization. *Ore Geol. Rev.* **2021**, *133*, No. 104081.

(7) Zhao, L.; Dai, S.; Nechaev, V. P.; Nechaeva, E. V.; Graham, I. T.; French, D. Enrichment origin of critical elements (Li and rare earth elements) and a Mo-U-Se-Re assemblage in Pennsylvanian anthracite from the Jincheng Coalfield, southeastern Qinshui Basin, northern China. *Ore Geol. Rev.* **2019**, *115*, No. 103184.

(8) Wang, Z.; Dai, S.; Zou, J.; French, D.; Graham, I. T. Rare earth elements and yttrium in coal ash from the Luzhou power plant in Sichuan, Southwest China: Concentration, characterization and optimized extraction. *Int. J. Coal Geol.* **2019**, *203*, 1−14.

(9) Li, B.; Zhuang, X.; Querol, X.; Moreno, N.; Córdoba, P.; Shangguan, Y.; Yang, L.; Li, J.; Zhang, F. Geological controls on the distribution of REY-Zr (Hf)-Nb (Ta) enrichment horizons in late Permian coals from the Qiandongbei Coalfield, Guizhou Province, SW China. *Int. J. Coal Geol.* **2020**, *231*, No. 103604.

(10) Seredin, V. V.; Dai, S.; Sun, Y.; Chekryzhov, I. Y. Coal deposits as promising sources of rare metals for alternative power and energy-efficient technologies. *Appl. Geochem.* **2013**, *31*, 1−11.

(11) Seredin, V. V.; Dai, S. Coal deposits as potential alternative sources for lanthanides and yttrium. *Int. J. Coal Geol.* **2012**, *94*, 67−93.

(12) Dai, S.; Wang, X.; Seredin, V. V.; Hower, J. C.; Ward, C. R.; O'Keefe, J. M. K.; Huang, W.; Li, T.; Li, X.; Liu, H.; Xue, W.; Zhao, L. Petrology, mineralogy, and geochemistry of the Ge-rich coal from the Wulantuga Ge ore deposit, Inner Mongolia, China: New data and genetic implications. *Int. J. Coal Geol.* **2012**, *90−91*, 72−99.

(13) Dai, S.; Wang, P.; Ward, C. R.; Tang, Y.; Song, X.; Jiang, J.; Hower, J. C.; Li, T.; Seredin, V. V.; Wagner, N. J.; Jiang, Y.; Wang, X.; Liu, J. Elemental and mineralogical anomalies in the coal-hosted Ge ore deposit of Lincang, Yunnan, southwestern China: Key role of N2−CO2-mixed hydrothermal solutions. *Int. J. Coal Geol.* **2015**, *152*, 19−46.

(14) Finkelman, R. B.; Palmer, C. A.; Wang, P. Quantification of the modes of occurrence of 42 elements in coal. *Int. J. Coal Geol.* **2018**, *185*, 138−160.

(15) Dai, S.; Ren, D.; Chou, C.-L.; Finkelman, R. B.; Seredin, V. V.; Zhou, Y. Geochemistry of trace elements in Chinese coals: A review of abundances, genetic types, impacts on human health, and industrial utilization. *Int. J. Coal Geol.* **2012**, *94*, 3−21.

(16) Luo, K.; Ren, D.; Xu, L.; Dai, S.; Cao, D.; Feng, F.; Tan, J. Fluorine content and distribution pattern in Chinese coals. *Int. J. Coal Geol.* **2004**, *57*, 143−149.

(17) Silva, L. F.; Jasper, A.; Andrade, M. L.; Sampaio, C. H.; Dai, S.; Li, X.; Li, T.; Chen, W.; Wang, X.; Liu, H.; Zhao, L.; Hopps, S. G.; Jewell, R. F.; Hower, J. C. Applied investigation on the interaction of hazardous elements binding on ultrafine and nanoparticles in Chinese anthracite-derived fly ash. *Sci. Total Environ.* **2012**, *419*, 250−264.

(18) Seredin, V. V.; Finkelman, R. B. Metalliferous coals: A review of the main genetic and geochemical types. *Int. J. Coal Geol.* **2008**, *76*, 253−289.

(19) Dai, S.; Zou, J.; Jiang, Y.; Ward, C. R.; Wang, X.; Li, T.; Xue, W.; Liu, S.; Tian, H.; Sun, X.; Zhou, D. Mineralogical and geochemical compositions of the Pennsylvanian coal in the Adaohai Mine, Daqingshan Coalfield, Inner Mongolia, China: Modes of occurrence and origin of diaspore, gorceixite, and ammonian illite. *Int. J. Coal Geol.* **2012**, *94*, 250−270.

(20) Permana, A. K.; Ward, C. R.; Li, Z.; Gurba, L. W. Distribution and origin of minerals in high-rank coals of the South Walker Creek area, Bowen Basin, Australia. *Int. J. Coal Geol.* **2013**, *116−117*, 185−207.

(21) Zhao, L.; Ward, C. R.; French, D.; Graham, I. T.; Dai, S.; Yang, C.; Xie, P.; Zhang, S. Origin of a kaolinite-NH 4 -illite-pyrophyllite-chlorite assemblage in a marine-influenced anthracite and associated strata from the Jincheng Coalfield, Qinshui Basin, Northern China. *Int. J. Coal Geol.* **2018**, *185*, 61−78.

https://doi.org/10.1021/acsomega.2c02062
ACS Omega 2022, 7, 18969−18984

(22) Zhou, M.; Dai, S.; Wang, Z.; Spiro, B. F.; Vengosh, A.; French, D.; Graham, I. T.; Zhao, F.; Zuo, J.; Zhao, J. The Sr isotope signature of Wuchiapingian semi-anthracites from Chongqing, southwestern China: Indication for hydrothermal effects. *Gondwana Res.* **2021**, *103*, 522−541.
(23) Dai, S.; Xie, P.; Jia, S.; Ward, C. R.; Hower, J. C.; Yan, X.; French, D. Enrichment of U-Re-V-Cr-Se and rare earth elements in the Late Permian coals of the Moxinpo Coalfield, Chongqing, China: Genetic implications from geochemical and mineralogical data. *Ore Geol. Rev.* **2017**, *80*, 1−17.
(24) China National Administration of Coal Geology. *Sedimentary Environments and Coal Accumulation of Late Permian Coal Formation in Western Guizhou, Southern Sichuan and Eastern Yunnan, China*; Chongqing University Press: Chongqing, 1996.
(25) Qin, S.; Gao, K.; Sun, Y.; Wang, J.; Zhao, C.; Li, S.; Lu, Q. Geochemical Characteristics of Rare-Metal, Rare-Scattered, and Rare-Earth Elements and Minerals in the Late Permian Coals from the Moxinpo Mine, Chongqing, China. *Energy Fuels* **2018**, *32*, 3138−3151.
(26) Zou, J.; Liu, D.; Tian, H.; Li, T.; Liu, F.; Tan, L. Anomaly and geochemistry of rare earth elements and yttrium in the late Permian coal from the Moxinpo mine, Chongqing, southwestern China. *Int. J. Coal Sci. Technol.* **2014**, *1*, 23−30.
(27) Zou, J.; Han, F.; Li, T.; Tian, H.; Li, Y. Mineralogical and Geochemical Compositions of the Lopingian Coals in the Zhongliangshan Coalfield, Southwestern China. *Minerals* **2018**, *8*, 104.
(28) Dai, S.; Wang, X.; Chen, W.; Li, D.; Chou, C.-L.; Zhou, Y.; Zhu, C.; Li, H.; Zhu, X.; Xing, Y.; Zhang, W.; Zou, J. A high-pyrite semianthracite of Late Permian age in the Songzao Coalfield, southwestern China: Mineralogical and geochemical relations with underlying mafic tuffs. *Int. J. Coal Geol.* **2010**, *83*, 430−445.
(29) ASTM D3173-11. *Standard Test Method for Moisture in the Analysis Sample of Coal and Coke*; In West Conshohocken, PA, 2011.
(30) ASTM D3174-11. *Standard Test Method for Ash in the Analysis Sample of Coal and Coke from Coal*; In West Conshohocken, PA, 2011.
(31) ASTM D3175-11. *Standard Test Method for Volatile Matter in the Analysis Sample of Coal and Coke*; In West Conshohocken, PA, 2011.
(32) ASTM D3177-02. *Standard Test Methods for Total Sulfur in the Analysis Sample of Coal and Coke*; In West Conshohocken, PA, 2007.
(33) ASTM D2492-02. *Standard Test Method for Forms of Sulfur in Coal*; In West Conshohocken, PA, 2007.
(34) Zou, J.; Cheng, L.; Guo, Y.; Wang, Z.; Tian, H.; Li, T. Mineralogical and Geochemical Characteristics of Lithium and Rare Earth Elements in High-Sulfur Coal from the Donggou Mine, Chongqing, Southwestern China. *Minerals* **2020**, *10*, 627.
(35) Li, X.; Dai, S.; Zhang, W.; Li, T.; Zheng, X.; Chen, W. Determination of As and Se in coal and coal combustion products using closed vessel microwave digestion and collision/reaction cell technology (CCT) of inductively coupled plasma mass spectrometry (ICP-MS). *Int. J. Coal Geol.* **2014**, *124*, 1−4.
(36) ASTM D5987-96. *Standard Test Method for Total Fluorine in Coal and Coke by Pyrohydrolytic Extraction and Ion Selective Electrode or Ion Chromatograph Methods*; In West Conshohocken, PA, 2007.
(37) ASTM D388-12. *Standard Classification of Coals by Rank*. In West Conshohocken, PA, 2012.
(38) Meng, L.; Qi, B.; Zou, J.; Cheng, J. Research on distribution and metamophic law of coal sorts in Late Permian in Chongqing area. *Coal Sci. Technol. Mag.* **2014**, *40*, 30−35. (in Chinese with English abstract)
(39) *China National Standardizing Committee, Classification for Quality of Coal. Part 1: Ash*; In Beijing, China, 2010 (in Chinese).
(40) *China National Standardizing Committee, Classification for Quality ofCoal. Part 2: Sulfur Content*; In Beijing, China, 2010 (in Chinese).
(41) Liu, J.; Nechaev, V. P.; Dai, S.; Song, H.; Nechaeva, E. V.; Jiang, Y.; Graham, I. T.; French, D.; Yang, P.; Hower, J. C. Evidence for multiple sources for inorganic components in the Tucheng coal deposit, western Guizhou, China and the lack of critical-elements. *Int. J. Coal Geol.* **2020**, *223*, No. 103468.
(42) Liu, J.; Song, H.; Dai, S.; Nechaev, V. P.; Graham, I. T.; French, D.; Nechaeva, E. V. Mineralization of REE-Y-Nb-Ta-Zr-Hf in Wuchiapingian coals from the Liupanshui Coalfield, Guizhou, southwestern China: Geochemical evidence for terrigenous input. *Ore Geol. Rev.* **2019**, *115*, No. 103190.
(43) Juster, T. C.; Brown, P. E.; Bailey, S. W. NH4-bearing illite in very low grade metamorphic rocks associated with coal, northeastern Pennsylvania. *Am. Mineral.* **1987**, *72*, 555−565.
(44) Dai, S.; Chou, C. L. Occurrence and origin of minerals in a chamosite-bearing coal of Late Permian age, Zhaotong, Yunnan, China. *Am. Mineral.* **2007**, *92*, 1253−1261.
(45) Tang, X.; Huang, W., *Trace elements in Chinese coals*; The Commercial Press: Beijing, 2004.
(46) Dai, S.; Tian, L.; Chou, C.-L.; Zhou, Y.; Zhang, M.; Zhao, L.; Wang, J.; Yang, Z.; Cao, H.; Ren, D. Mineralogical and compositional characteristics of Late Permian coals froman area of high lung cancer rate in Xuan Wei, Yunnan, China: Occurrence and origin of quartz and chamosite. *Int. J. Coal Geol.* **2008**, *76*, 318−327.
(47) Zhou, M.; Zhao, L.; Wang, X.; Nechaev, V. P.; French, D.; Spiro, B. F.; Graham, I. T.; Hower, J. C.; Dai, S. Mineralogy and geochemistry of the Late Triassic coal from the Caotang mine, northeastern Sichuan Basin, China, with emphasis on the enrichment of the critical element lithium. *Ore Geol. Rev.* **2021**, *139*, No. 104582.
(48) Zhao, L.; Ward, C. R.; French, D.; Graham, I. T. Mineralogical composition of Late Permian coal seams in the Songzao Coalfield, southwestern China. *Int. J. Coal Geol.* **2013**, *116−117*, 208−226.
(49) Dai, S.; Zhou, Y.; Ren, D.; Wang, X.; Li, D.; Zhao, L. Geochemistry and mineralogy of the Late Permian coals from the Songzo Coalfield, Chongqing, southwestern China. *Sci. China, Ser. D: Earth Sci.* **2007**, *50*, 678−688.
(50) Chen, J.; Chen, P.; Yao, D.; Liu, Z.; Wu, Y.; Liu, W.; Hu, Y. Mineralogy and geochemistry of Late Permian coals from the Donglin Coal Mine in the Nantong coalfield in Chongqing, southwestern China. *Int. J. Coal Geol.* **2015**, *149*, 24−40.
(51) Chou, C.-L. Sulfur in coals: A review of geochemistry and origins. *Int. J. Coal Geol.* **2012**, *100*, 1−13.
(52) Wang, P.; Ji, D.; Yang, Y.; Zhao, L. Mineralogical compositions of Late Permian coals from the Yueliangtian mine, western Guizhou, China: Comparison to coals from eastern Yunnan, with an emphasis on the origin of the minerals. *Fuel* **2016**, *181*, 859−869.
(53) Dai, S.; Seredin, V. V.; Ward, C. R.; Hower, J. C.; Xing, Y.; Zhang, W.; Song, W.; Wang, P. Enrichment of U−Se−Mo−Re−V in coals preserved within marine carbonate successions: geochemical and mineralogical data from the Late Permian Guiding Coalfield, Guizhou, China. *Miner. Deposita* **2015**, *50*, 159−186.
(54) Ketris, M. P.; Yudovich, Y. E. Estimations of Clarkes for Carbonaceous biolithes: World averages for trace element contents in black shales and coals. *Int. J. Coal Geol.* **2009**, *78*, 135−148.
(55) Taylor, S. R.; Mclennan, S. H. *The continental Crust: Its Composition and Evolution*; Blackwell: Oxford, 1985.
(56) Grigoriev, N. A. *Chemical Element Distribution in the Upper Continental Crust*; UB RAS: Ekaterinburg, 2009.
(57) Dai, S.; Ren, D.; Ma, S. The cause of endemic fluorosis in western Guizhou Province, Southwest China. *Fuel* **2004**, *83*, 2095−2098.
(58) Zheng, B.; Ding, Z.; Huang, R.; Zhu, J.-M.; Yu, X.; Wang, A.; Zhou, D.; Mao, D.; Su, H. Issues of health and disease relating to coal use in southwestern China. *Int. J. Coal Geol.* **1999**, *40*, 119−132.
(59) Ando, M.; Tadano, M.; Yamamoto, S.; Tamura, K.; Asanuma, S.; Watanabe, T.; Kondo, T.; Sakurai, S.; Ji, H.; Liang, C.; Chen, X.; Hong, Z.; Cao, S. Health effects of fluoride pollution caused by coal burning. *Sci. Total Environ.* **2001**, *271*, 107−116.
(60) Wu, D. *Environmental geochemistry of fluorine in Chinese coal*; Institute of Geochemistry, CAS: Guiyang, 2004.
(61) Xiong, Y.; Xiao, T.; Liu, Y.; Zhu, J.; Ning, Z.; Xiao, Q. Occurrence and mobility of toxic elements in coals from endemic

https://doi.org/10.1021/acsomega.2c02062
ACS Omega 2022, 7, 18969−18984

fluorosis areas in the Three Gorges Region, SW China. *Ecotoxicol. Environ. Saf.* **2017**, *144*, 1−10.
(62) Dai, S.; Graham, I. T.; Ward, C. R. A review of anomalous rare earth elements and yttrium in coal. *Int. J. Coal Geol.* **2016**, *159*, 82−95.
(63) Yan, X.; Dai, S.; Graham, I. T.; He, X.; Shan, K.; Liu, X. Determination of Eu concentrations in coal, fly ash and sedimentary rocks using a cation exchange resin and inductively coupled plasma mass spectrometry (ICP-MS). *Int. J. Coal Geol.* **2018**, *191*, 152−156.
(64) He, B.; Xu, Y.-G.; Zhong, Y.-T.; Guan, J.-P. The Guadalupian−Lopingian boundary mudstones at Chaotian (SW China) are clastic rocks rather than acidic tuffs: Implication for a temporal coincidence between the end-Guadalupian mass extinction and the Emeishan volcanism. *Litho* **2010**, *119*, 10−19.
(65) Xiao, L.; Xu, Y. G.; Mei, H. J.; Zheng, Y. F.; He, B.; Pirajno, F. Distinct mantle sources of low-Ti and high-Ti basalts from the western Emeishan large igneous province, SW China: implications for plume−lithosphere interaction. *Earth Planet. Sci. Lett.* **2004**, *228*, 525−546.
(66) Chung, S.-L.; Jahn, B.-M. Plume-lithosphere interaction in generation of the Emeishan flood basalts at the Permian-Triassic boundary. *Geology* **1995**, *23*, 889.
(67) Zhuang, X.; Querol, X.; Zeng, R.; Xu, W.; Alastuey, A.; Lopez-Soler, A.; Plana, F. Mineralogy and geochemistry of coal from the Liupanshui mining district, Guizhou, south China. *Int. J. Coal Geol.* **2000**, *45*, 21−37.
(68) Zhuang, X.; Su, S.; Xiao, M.; Li, J.; Alastuey, A.; Querol, X. Mineralogy and geochemistry of the Late Permian coals in the Huayingshan coal-bearing area, Sichuan Province, China. *Int. J. Coal Geol.* **2012**, *94*, 271−282.
(69) Wang, X.; Dai, S.; Chou, C.-L.; Zhang, M.; Wang, J.; Song, X.; Wang, W.; Jiang, Y.; Zhou, Y.; Ren, D. Mineralogy and geochemistry of Late Permian coals from the Taoshuping Mine, Yunnan Province, China: Evidences for the sources of minerals. *Int. J. Coal Geol.* **2012**, *96*−*97*, 49−59.
(70) Dai, S.; Liu, J.; Ward, C. R.; Hower, J. C.; French, D.; Jia, S.; Hood, M. M.; Garrison, T. M. Mineralogical and geochemical compositions of Late Permian coals and host rocks from the Guxu Coalfield, Sichuan Province, China, with emphasis on enrichment of rare metals. *Int. J. Coal Geol.* **2016**, *166*, 71−95.
(71) Dai, S.; Luo, Y.; Seredin, V. V.; Ward, C. R.; Hower, J. C.; Zhao, L.; Liu, S.; Zhao, C.; Tian, H.; Zou, J. Revisiting the late Permian coal from the Huayingshan, Sichuan, southwestern China: Enrichment and occurrence modes of minerals and trace elements. *Int. J. Coal Geol.* **2014**, *122*, 110−128.
(72) Hayashi, K. I.; Fujisawa, H.; Holland, H. D.; Ohmoto, H. Geochemistry of ∼ 1.9 Ga sedimentary rocks from northeastern Labrador, Canada. *Geochim. Cosmochim. Acta* **1997**, *21*, 4115−4137.
(73) Hower, J.; Eble, C.; O'Keefe, J.; Dai, S.; Wang, P.; Xie, P.; Liu, J.; Ward, C.; French, D. Petrology, Palynology, and Geochemistry of Gray Hawk Coal (Early Pennsylvanian, Langsettian) in Eastern Kentucky, USA. *Minerals* **2015**, *5*, 592−622.
(74) Zheng, X.; Dai, S.; Nechaev, V.; Sun, R. Environmental perturbations during the latest Permian: Evidence from organic carbon and mercury isotopes of a coal-bearing section in Yunnan Province, southwestern China. *Chem. Geol.* **2020**, *549*, No. 119680.
(75) Zhou, Y.; Ren, Y. Distribution of arsenic in coals of Yunnan Province, China, and its controlling factors. *Int. J. Coal Geol.* **1992**, *20*, 85−98.
(76) Dai, S.; Li, T.; Seredin, V. V.; Ward, C. R.; Hower, J. C.; Zhou, Y.; Zhang, M.; Song, X.; Song, W.; Zhao, C. Origin of minerals and elements in the Late Permian coals, tonsteins, and host rocks of the Xinde Mine, Xuanwei, eastern Yunnan, China. *Int. J. Coal Geol.* **2014**, *121*, 53−78.
(77) Xie, P.; Zhang, S.; Wang, Z.; Wang, L.; Xu, Y. Geochemical characteristics of the Late Permian coals from the Yueliangtian Coalfield, western Guizhou, southwestern China. *Arabian J. Geosci.* **2017**, *10*, 5.
(78) Daniels, E. J.; Altaner, S. P. Clay mineral authigenesis in coal and shale from the anthracite region, Pennsylvania. *Am. Mineral.* **1990**, *75*, 825−839.
(79) Daniels, E. J.; Aronson, J. L.; Altaner, S. P.; Clauer, N. Late Permian age of NH4-bearing illite in anthracite from eastern Pennsylvania: Temporal limits on coalification in the central Appalachians. *GSA Bull.* **1994**, *106*, 760−766.
(80) Susilawati, R.; Ward, C. R. Metamorphism of mineral matter in coal from the Bukit Asam deposit, south Sumatra, Indonesia. *Int. J. Coal Geol.* **2006**, *68*, 171−195.
(81) Ward, C. R.; Christie, P. J. Clays and other minerals in coal seams of the Moura-Baralaba area, Bowen Basin, Australia. *Int. J. Coal Geol.* **1994**, *25*, 287−309.
(82) Xie, P.; Dai, S.; Hower, J. C.; Nechaev, V. P.; French, D.; Graham, I. T.; Wang, X.; Zhao, L.; Zuo, J. Nitrogen isotopic compositions in NH4+-mineral-bearing coal: Origin and isotope fractionation. *Chem. Geol.* **2021**, *559*, No. 119946.
(83) Hatch, J. R.; Gluskoter, H. J.; Lindahl, P. C. Sphalerite in coals from the Illinois Basin. *Econ. Geol.* , *71*, 613−624, DOI: 10.2113/gsecongeo.71.3.613.
(84) Shand, P.; Johannesson, K. H.; Chudaev, O.; Chudaeva, V.; Edmunds, W. M. *Rare earth element contents of high pCO2 groundwaters of Primorye, Russia: mineral stability and complexation controls*; Springer: The Netherlands, 2005.
(85) Sichuan Bureau of Coal Geology; Sichuan Institute of Geology. *Sedimentary environment and accumulating rule of Late Permian coal-bearing sequences in southern Sichuan*; Guizhou Science and Technology Press: Guiyang, 1993 (in Chinese).
(86) Li, C.; Xiao, J. The application of trace element to the study on paleosalinities in Shahejie Formation of Dongying Basin Shengli Oilfield. *Acta Sedimentol. Sin.* **1988**, *6*, 100−107. (in Chinese with English abstract)
(87) Dai, S.; Finkelman, R. B. Coal as a promising source of critical elements: Progress and future prospects. *Int. J. Coal Geol.* **2018**, *186*, 155−164.
(88) Zhang, W.; Honaker, R. Characterization and recovery of rare earth elements and other critical metals (Co, Cr, Li, Mn, Sr, and V) from the calcination products of a coal refuse sample. *Fuel* **2020**, *267*, No. 117236.
(89) Gollakota, A. R. K.; Volli, V.; Shu, C. M. Progressive utilisation prospects of coal fly ash: A review. *Sci. Total Environ.* **2019**, *672*, 951−989.
(90) Clint, S.; Kolker, A. *Rare Earth Elements in Coal and Coal Fly Ash*; U.S. Geological Survey: Reston, VA, 2019.
(91) Lin, R.; Stuckman, M.; Howard, B.; Bank, T.; Roth, E.; Macala, M. K.; Lopano, C.; Soong, Y.; Granite, E. Application of sequential extraction and hydrothermal treatment for characterization and enrichment of rare earth elements from coal fly ash. *Fuel* **2018**, *232*, 124−133.
(92) Hower, J.; Groppo, J.; Henke, K.; Hood, M.; Eble, C.; Honaker, R.; Zhang, W.; Qian, D. Notes on the Potential for the Concentration of Rare Earth Elements and Yttrium in Coal Combustion Fly Ash. *Minerals* **2015**, *5*, 356−366.
(93) Dai, S.; Zhang, W.; Ward, C. R.; Seredin, V. V.; Hower, J. C.; Li, X.; Song, W.; Wang, X.; Kang, H.; Zheng, L.; Wang, P.; Zhou, D. Mineralogical and geochemical anomalies of Late Permian coals from the Fusui Coalfield, Guangxi Province, southern China: influences of terrigenous materials and hydrothermal fluids. *Int. J. Coal Geol.* **2013**, *105*, 60−84.

https://doi.org/10.1021/acsomega.2c02062
ACS Omega 2022, 7, 18969−18984